International Scientific-Technical and Production Journal

The Paton WELDING JOURNAL

December 2008 # 12

English translation of the monthly «Avtomaticheskaya Svarka» (Automatic Welding) journal published in Russian since 1948

Founders: *E.O. Paton Electric Welding Institute of the NAS of Ukraine*
International Association «Welding»

Publisher: *International Association «Welding»*

Address:
E.O. Paton Electric Welding Institute,
International Association «Welding»,
11, Bozhenko str., 03680, Kyiv, Ukraine
Tel.: (38044) 287 67 57
Fax: (38044) 528 04 86
E-mail: journal@paton.kiev.ua
http://www.nas.gov.ua/pwj

State Registration Certificate
KV 4790 of 09.01.2001

Subscriptions:
$324, 12 issues per year,
postage and packaging included.
Back issues available.

CONTENTS

APPLICATION OF NANOTECHNOLOGY OF PERMANENT JOINING OF ADVANCED LIGHT-WEIGHT METALLIC MATERIALS FOR AEROSPACE ENGINEERING

B.E. PATON, A.Ya. ISHCHENKO and **A.I. USTINOV**
E.O. Paton Electric Welding Institute, NASU, Kiev, Ukraine

The paper deals with the possibility of making solid-phase joints of advanced structural quasi-crystalline and intermetallic alloys, aluminium composites and nanomaterials by diffusion and friction stir welding using nanostructured fillers. It is shown that these welding processes allow producing permanent joints of difficult-to-weld materials applied in fabrication of aerospace products, parts of gas turbine engines, electrical engineering and heat exchanger units, in repair and restoration operations.

Keywords: aluminium alloys, aluminium composites, quasi-crystalline alloys, intermetallic materials, weldability, permanent joint, solid-phase joint, self-propagating high-temperature synthesis, diffusion welding, friction stir welding, nanostructure, mechanical properties, welded structures, aerospace engineering

At the start of the XXI century it has become necessary to cardinally improve the scientific-technical level of economics all over the world. Solving this problem requires conducting extensive research, as well as mass introduction of advanced technologies into production. According to the predictions of many competent organizations, development of nanomaterials and nanotechnologies is a high priority. These are exactly the materials and technologies which, alongside others, will promote an essential improvement of productive efficiency in such spheres as mechanical engineering, power engineering, construction, agriculture, medicine, etc.

By now new light aluminium alloys and composite materials with extraordinary properties due to the quasicrystalline or nanodispersed structure of semi-finished products have already been developed for fabrication of aerospace engineering structures [1, 2]. It should be noted that with regular welding processes, metallic materials are heated to a temperature, which results in their melting or activation of diffusion processes in the joint zone. In the case of application of nanostructured composite materials, alloys based on intermetallics or other high alloys heating up to a high temperature leads to irreversible structural transformations [3] and degradation of the initial physico-mechanical properties of the material [4]. In this connection, an urgent problem is lowering of temperature and reduction of the duration of weld formation process in order to preserve the initial structure and level of material properties in the joint zone. Among the diverse currently available welding processes those of solid-phase joining, i.e. without metal melting, should be more widely accepted. These include, primarily, diffusion welding and friction stir welding [5].

The idea of solving such a problem, on the whole, is based on that the temperature of the solid-phase joining process can be reduced, if rapidly crystallized-amorphized homogeneous strips [6] or composite thin-film materials with a nanolayered structure [1] are used as welding fillers. In such materials the non-equilibrium state of the fine structure leads to an essential lowering of temperature, at which the diffusion processes are running intensively. Formation of sound joints is promoted by application of multilayered nanostructured films, consisting of metals entering into an exothermal reaction of intermetallic synthesis.

Let us consider a number of specific examples of nanolayered filler application and the results of PWI work in this field for light materials for aerospace applications.

For solid-phase joining of high-temperature materials, including intermetallic alloys, thin nanostructured foils from multilayered compositions of various metal elements of Ti / Al, Ni / Al, Cu / Al, etc. have been developed and are used as welding fillers. Their manufacture is based on the process of layer-by-layer consolidation of elements from the vapour phase, using electron beam vacuum technology (Figure 1). The deposition technology enables adjustment of the process of layered structure formation in a broad range of thicknesses of individual layers ---- from several nanometers up to tens of micrometers (Figure 2, *a*).

At heating the nanostructured foils are prone to development of the reaction of self-propagating high-temperature synthesis (SPHTS) of intermetallic compounds, which runs very quickly and is characterized by exothermal effect. The necessary condition for joining materials without melting due to activation of diffusion processes in the solid state is a stable running of SPHTS reaction. As shown by experience, this requires application of multilayer foils of more than 30 μm thickness (Figure 2, *b*).

Diffusion bonding of microdispersed high-strength aluminium composite of AMg5 + 27 % Al_2O_3 system with application of interlayers from nanostructured multilayer foils turned out to be more effective than arc welding [4]. The metal matrix of this

material contains a large quantity of the strengthening phase in the form of insoluble particles of aluminium oxide, and, therefore, it is difficult to treat and to weld. Figure 3, *a* shows the structure of the composite in the initial condition, differing by a set of valuable properties, namely high specific modulus of elasticity, room and higher temperature strength, wear resistance, low coefficient of linear expansion. This material is widely applied in products for aerospace and transportation engineering.

Performance of fusion welding of the considered aluminium composite is difficult in view of the increased viscosity of weld pool metal and susceptibility of reinforcing Al_2O_3 particles to agglomeration. The strengthening particle conglomerates forming in the welds lower the strength and corrosion resistance of the produced joints [7]. In diffusion welding at lower temperatures segregation of the strengthening phase particles and chemical reactions between the composite material components are practically absent. In this connection the solid-phase process of joining a microdispersed composite based on aluminium reinforced by Al_2O_3 ceramic particles is preferable [8]. Weld strength in regular diffusion welding using one-layer plastic aluminium foil does not exceed 50–60 % of base material strength (Figure 3, *b*).

For activisation of the diffusion welding process and improvement of weld strength, interlayers (fillers) from multilayered nanostructured foils of two types, namely Ti / Al and Cu / Al were used (Figure 4). The first of them was 60 to 150 μm thick at 50 to 150 nm thickness of the nickel and aluminium nanolayers and corresponded to the stoichiometric composition of Ni_3Al intermetallic, and the second, having approximately the same thickness, corresponded to the composition of Al + 33 % Cu eutectic [9].

It is established that replacement of regular aluminium interlayer (basic variant) by nanolayered condensate foil allows lowering the composite welding temperature by 80–100 °C, providing sound formation of the permanent joint at a lower welding pressure, which does not cause any noticeable macroplastic deformation in the welded materials. When Cu / Al foil is used, a complete dissolution of the filler in the joint zone is also noted (Figure 3, *c*, *d*). Weld metal strength increases up to the base metal level (Figure 5). Coefficient of joint strength is equal to 0.87 to 0.90.

Diffusion welding of intermetallic alloy based on γ-TiAl *titanium aluminide* using interlayers from multilayered nanostructured Ti / Al, Ni / Al, Ti / Ni foils is a practically real and effective method of joining advanced high-temperature materials [10–12]. As an example, let us consider Ti–48Al–2Nb–2Mn (at.%) intermetallic alloy operating at 700–1100 °C, i.e. much higher than the operating temperature of currently available titanium superalloys ($T \leq 600$ °C) [13]. This will enable application of the above alloy for gas turbine engines, flying vehicle skin, parts of load-carrying structures of aerospace engineering products, etc.

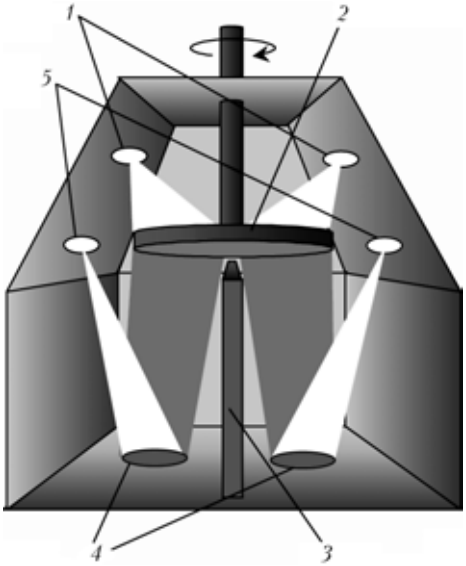

Figure 1. Schematic of the process of electron beam deposition of multilayered condensates: *1* — electron beam sources (guns) for heating; *2* — substrate; *3* — separating impermeable screen; *4* — crucibles for ingot evaporation; *5* — electron beam guns for evaporation

Alloys based on γ-TiAl are light (density of 3.8–4.0 g / cm^3) and resistant to oxidation at up to 900–1000 °C temperature. Their modulus of elasticity at room temperature is equal to 160–175 GPa, and at 900–1000 °C it decreases to 150 GPa. Industrial application of the above material is restrained by its low ductility at standard temperature (δ = 0.1–0.5 %). Semi-finished product treatability is made difficult by the high deformation resistance of the material.

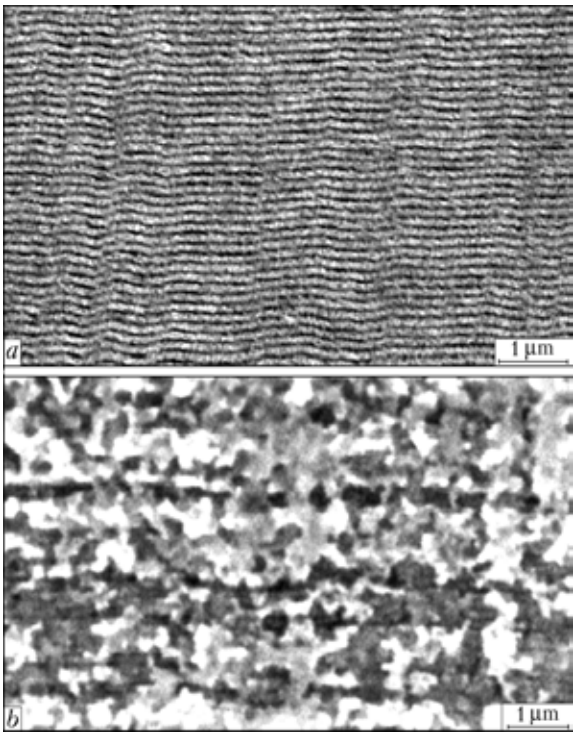

Figure 2. Microstructure of a multilayered nanostructured Ni / Al condensate, produced by electron beam vapour phase deposition in vacuum, in the initial condition (*a*) and after SPHTS reaction at the temperature of 500 °C (*b*)

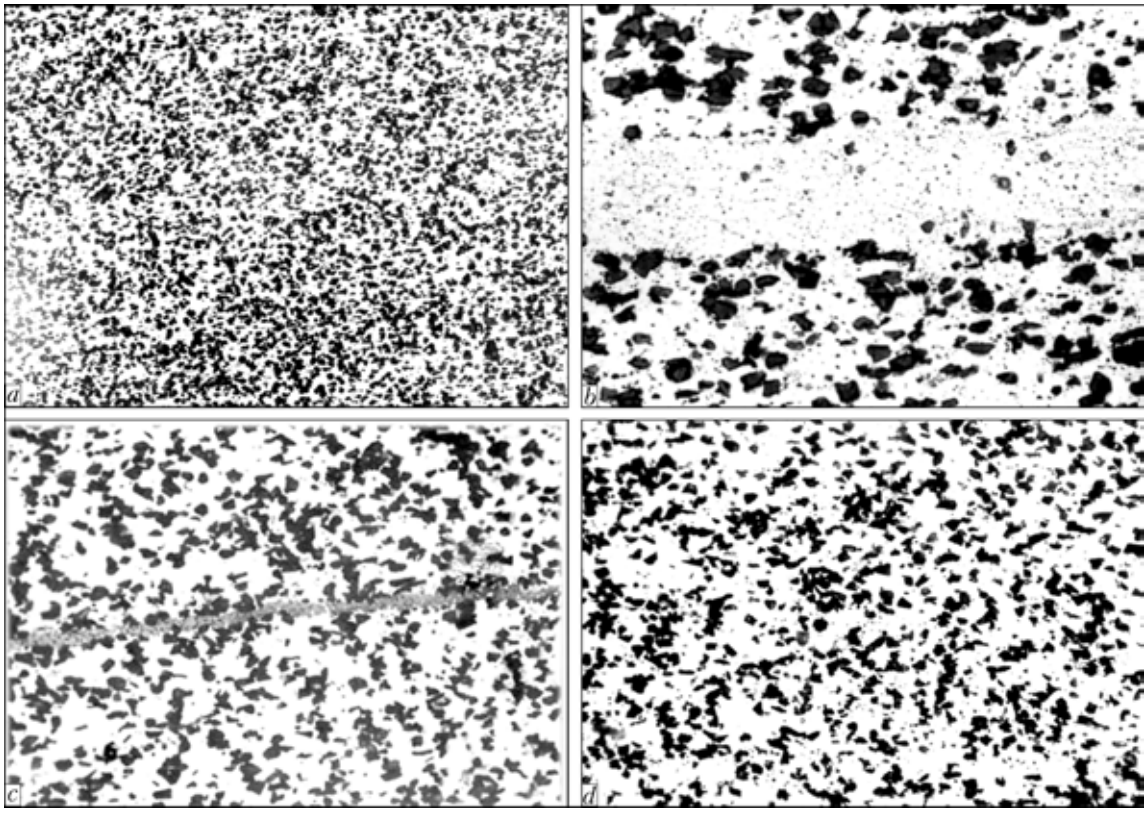

Figure 3. Microstructure of base metal — AMg5 + 27 % Al_2O_3 composite (*a*) and its permanent joints produced by diffusion welding using single-layer aluminium interlayer (*b*), as well as multilayered nanostructured foil corresponding to intermetallic composition of Ni_3Al (*c*) or eutectic composition of Al + 33 % Cu (*d*) (*a* — ×200; *b*–*d* — ×400)

In the initial condition Ti–48Al–2Nb–2Mn (at.%) alloy develops a fully lamellar structure, which is presented by practically equiaxed grains of 60–120 μm size with plates (lamels) of γ- and α-phase with different orientation within each grain. Dispersed inclusions with an increased niobium content uniformly distributed through the matrix volume, form against the background of the lamellar structure. Alloy microhardness is equal to 3000–4000 MPa.

Permanent joints of components from this material were made by diffusion welding in vacuum using multilayered Ti / Al, Ti / Ni, Ni / Al foils of the total thickness from 10 up to 20 μm by layer-by-layer deposition from the vapour phase of individual nanosized layers of the respective components using electron beam tech-

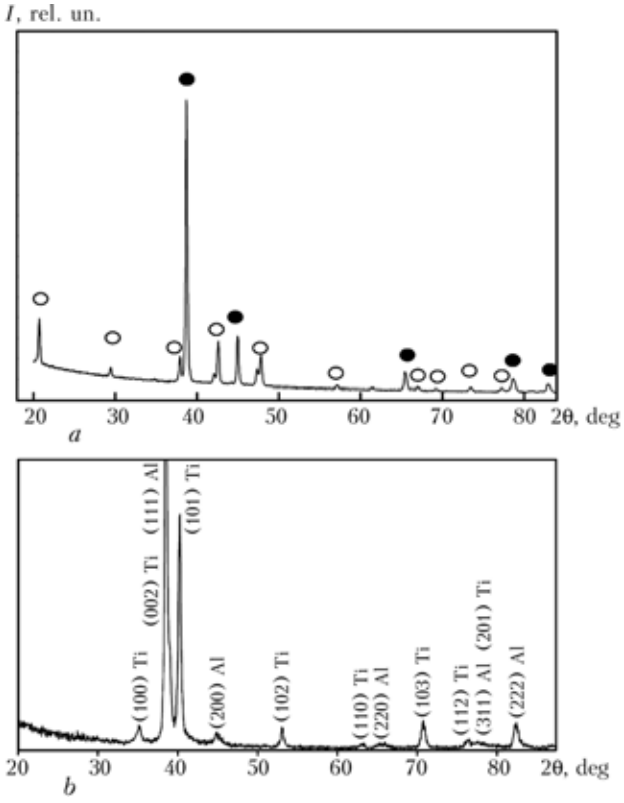

Figure 4. X-ray diffraction spectra of foils of γ-TiAl intermetallics (*a*) and nanodispersed eutectic composition Al + 33 % Cu (*b*): ● — Al; ❍ — Al_2Cu; *I* — radiation intensity; θ — angle of diffraction

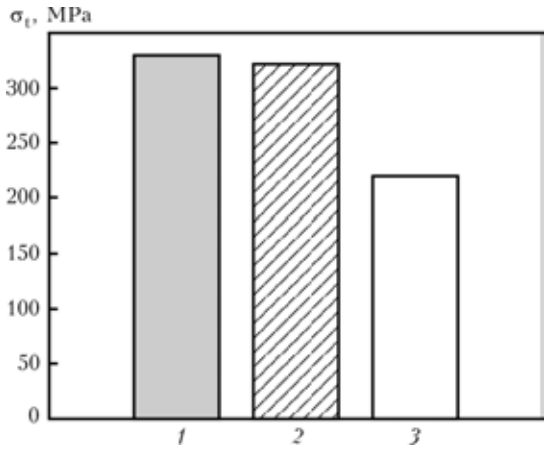

Figure 5. Tensile strength σ_t of base metal (*1*) and joints of AMg5 + 27 % Al_2O_3 aluminuim composite produced by diffusion welding using nanolayered foil of Al–Cu system (*2*) and single-layer aluminium strip (*3*)

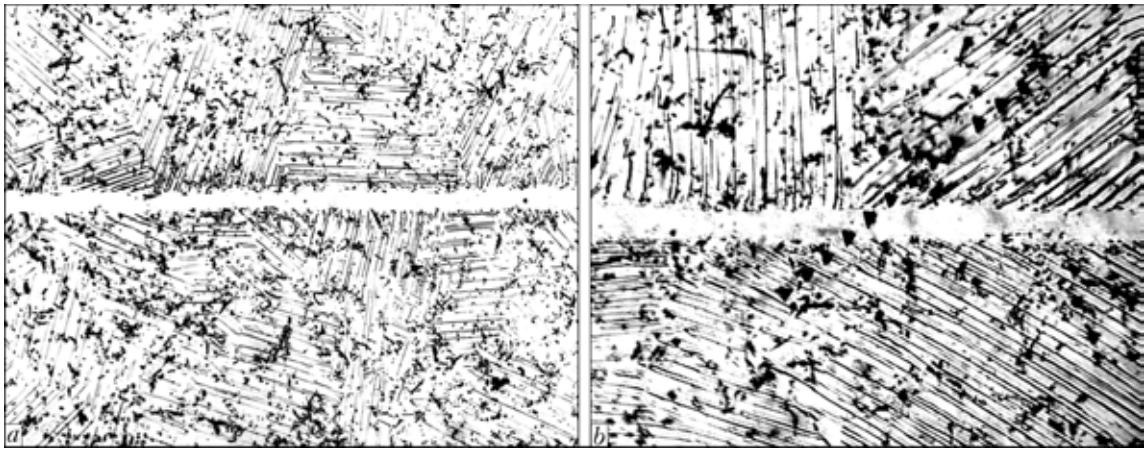

Figure 6. Microstructure of the joint zone of an alloy based on γ-TiAl intermetallics (Ti–48Al–2Nb–2Mn) produced by diffusion welding (temperature of 1200 °C) using nanolayered foil corresponding to γ-TiAl intermetallic compound in its composition (*a* — ×200; *b* — ×300): ▼ — diamond indentor imprints

nology. Welding was performed in U-394 unit designed for diffusion welding and fitted with circular electron beam heaters of blanks. Equivalent joints with a favourable structure were obtained using nanolayered Ti / Al foil of the total thickness of 20 μm in the following welding mode: welding temperature T_w = 1200 °C; welding time τ = 20 min; pressure P = = 45 MPa.

Metallographic analysis of the structure revealed a continuous uniform weld 15–18 μm wide (Figure 6, *a*), the metal of which corresponds to the main γ-TiAl intermetallic phase as to its composition (Figure 7). A fine-grain zone, formation of which is due to the recrystallization process, is revealed near the weld at 5–10 μm distance. Microhardness values of 3500–4200 MPa in the joint zone are close to analogous index of the base metal (3000–4000 MPa) in the initial condition, which is indicative of equivalent strength of the weld metal compared to base material (Figure 6, *b*).

When foils of Ni / Al and Ti / Ni systems are used, the joint zone develops structural components with microhardness 2–3 times higher than that of the base material —- Ti–48Al–2Nb–2Mn alloy (at.%). Increase of microhardness (Figure 8) can promote lowering of joint ductility.

The above confirms that vacuum diffusion welding using nanolayered Ti / Al foils allows producing sound homogeneous equivalent joints of Ti–48Al–2Nb–2Mn intermetallic alloy.

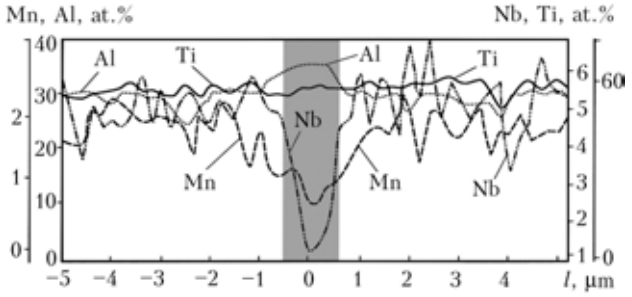

Figure 7. Nature of distribution of manganese, aluminium, niobium and titanium in the joint zone of an alloy based on γ-TiAl intermetallics (Ti–48Al–2Nb–2Mn) produced by diffusion welding at 1200 °C using nanolayered foil corresponding in its composition to γ-TiAl intermetallic compound: *l* — distance from weld axis

Friction stir welding of quasi-crystalline high-temperature alloy of Al–Fe–Cr–Ti system without fillers is an example of producing an original alloy with quasi-crystalline strengthening and a new friction stir welding process with layer-by-layer stirring of the weld metal (Figure 9, *a*). The weld metal structure and its mechanical properties are improved owing to intensive plastic deformation under the conditions of three-dimensional compression in friction stir welding.

High-temperature aluminium alloy based on Al–Fe–Cr–Ti system was in the form of extruded semi-finished products with a nanostructured matrix, formed at rapid solidification of the initial material in the form of finest granules (actually, powders) with particles of less than 100 μm size. Alloy strengthening is due to presence in its composition of nanosized quasi-crystalline intermetallic particles [14]. Intermetallic phases present in the above alloy composition, contain transition refractory elements, which strengthen the solid solution (aluminium matrix) and reduce the diffusion rate in it (Figures 10 and 11). Extruded semi-finished products are characterized by the following mechanical properties: $\sigma_{0.2}$ = 485 MPa, σ_t = 542 MPa, δ = 7 % (at room temperature), $\sigma_{0.2}$ = 283 MPa, σ_t = = 297 MPa, δ = 3.5 % (at 300 °C). The alloy belongs to a new material class designed for engineering applications in the case, when it is necessary to reduce the weight of a structure operating at increased (up

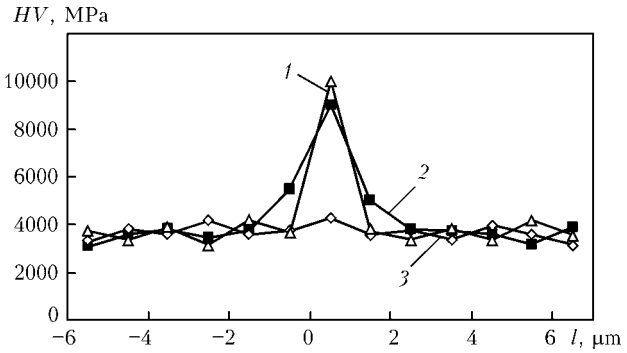

Figure 8. Nature of distribution of *HV* microhardness in the weld zone at diffusion welding of Ti–48Al–2Nb–2Mn intermetallic alloy with application of interlayers from nanolayered foils of different systems: *1* — Ni–Al; *2* — Ti–Ni; *3* — Ti–Al

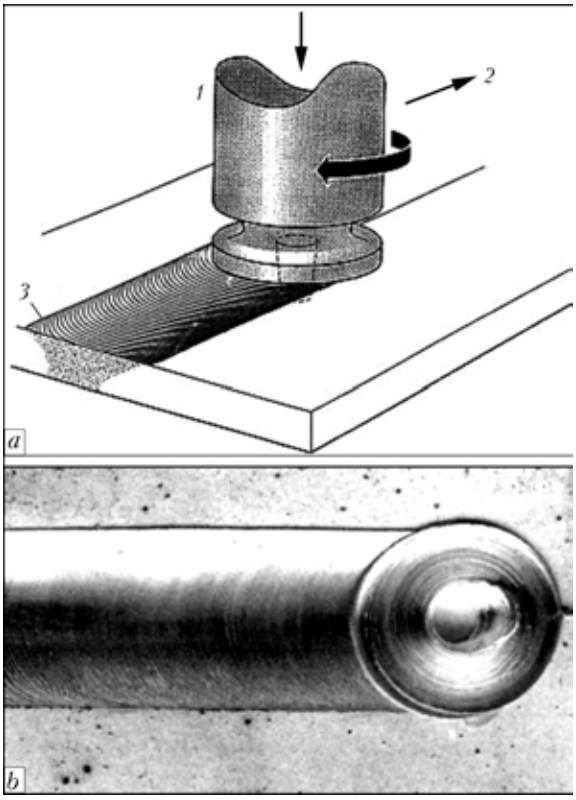

Figure 9. Schematic of friction stir welding of nanodispersed aluminium composite Al + 7 % Al_2O_3 (*a*) and weld appearance (*b*): *1* — rotating working tool; *2* — direction of tool displacement in welding; *3* — weld

to 300–400 °C) temperature and ensure sufficiently high specific strength. These requirements are urgent for many types of vehicle structures, for instance in aircraft and engine construction.

The results of investigation of friction stir welding and of the produced joint properties showed that the weld metal forms a more dispersed and uniform grain structure than in the base metal with the size of matrix $d \leq 300$ nm and quasi-crystal particles $d \leq 100$ nm, ultimate strength of the joints being 370 MPa.

Scanning electron beam microscopy revealed the specific nature of the structure of base metal and welds, which is formed under the conditions of intensive plastic deformation (Figure 12, *a*, *b*).

Friction stir welding of nanodispersed aluminium composite Al + Al_2O_3 without fillers is another example of acceptance of new developments by industry. Electron beam vapour-phase technology enables manufacturing compact billets of nanostructured material in the form of sheets [7, 15], and well as other shapes, typical for three-dimensional structures (cylindrical, conical, semi-spherical). Friction welding with multilayer stirring ensures their joining under the conditions, when base material properties are preserved to a great extent.

Experimental verification of this idea was started with welding of samples of sheet aluminium composite, reinforced by insoluble particles of Al_2O_3 oxide. Such a material operates at a higher temperature than do regular aluminium alloys.

Composite structure is characterized by columnar crystals directed normal to the flat sample surface (Figure 12, *c*, *d*). Oxide inclusions of the size of 10–50 nm, are uniformly distributed, particle spacing being 60–100 nm. Composite hardness is *HRB* 99–100 MPa, its strength being σ_t = 340 MPa.

Plates of nanodispersed Al + 7 % Al_2O_3 composite were joined by friction stir welding at the speed of 14 m / h, working tool rotation frequency being 1420 rpm. Figure 9, *b* gives the appearance of the produced weld. Metallographic studies showed that during welding transformation of columnar crystallites into equiaxed grains occurs in the joint zone, their size being reduced 3–5 times (Figure 12, *c*, *d*). Base metal hardness is equal to 680–700 MPa, that of weld metal being 780–900 MPa. Friction stir welding provides equivalent joints, owing to improved homogeneity and dispersed state of the structural constituents.

Thus, considered are the examples of joining difficult-to-weld regular and nanodispersed materials using nanostructured fillers in the form of strips, foils and films made by the method of layer-by-layer consolidation of metals from the vapour phase using electron beam technology. Thin foils from activated multilayered nanostructured compositions of Ti / Al, Ni / Al, Ni / Ti and other metals prone to SPHTS reaction of intermetallic compounds, have been devel-

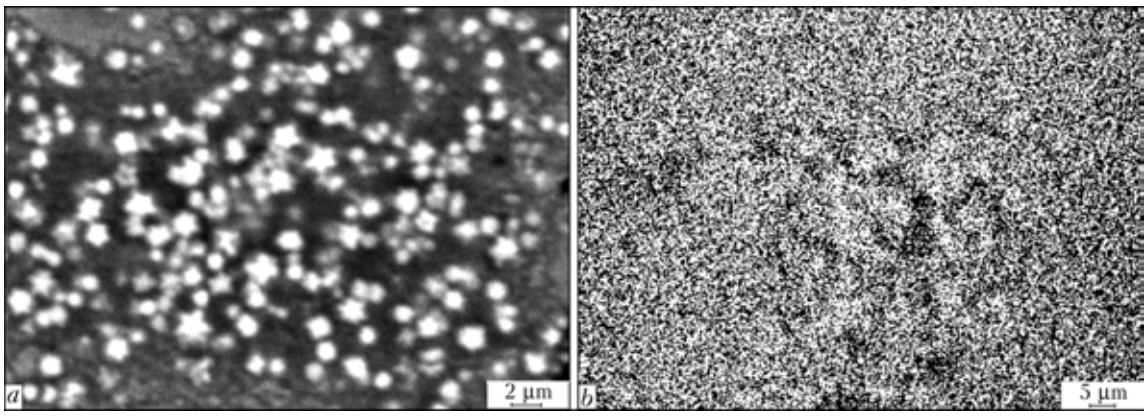

Figure 10. Quasicrystalline particles of intermetallic phase precipitating in rapidly solidified fine granules of Al–3Fe–3Cr alloy: *a*, *b* — images obtained by the method of scanning electron microscopy in back-scattered electrons, *a*, and characteristic X-ray radiation

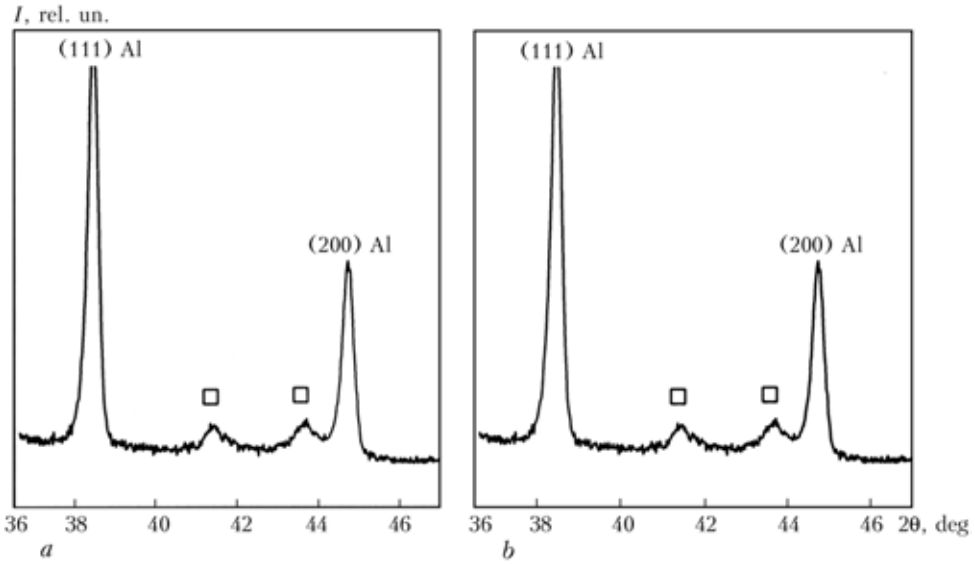

Figure 11. X-ray diffraction of fine granules of Al–3Fe–3Cr (*a*) and Al–2.5Fe–2.5Cr–0.5Ti–0.5Zr (at.%) alloys (*b*): ❒ — quasicrystalline phase

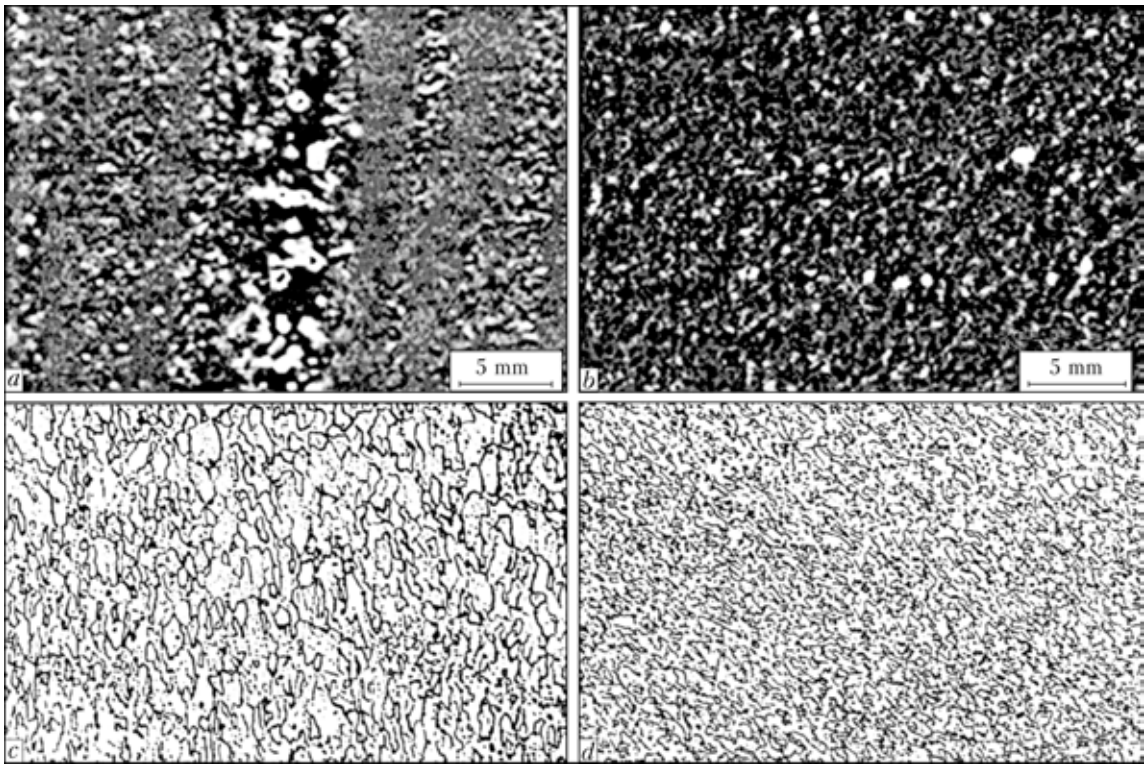

Figure 12. Microstructure of base metal (*a*, *c*) and weld metal (*b*, *d*) made by friction stir welding: *a*, *b* — extruded strip from quasicrystalline alloy of Al–Cr–Fe system; *c*, *d* — nanodispersed aluminium composite Al + 7 % Al_2O_3 (×400)

oped for their practical application in welding various metallic materials.

Advanced technologies of joining different kinds of nanostructured materials are realized using diffusion welding or friction stir welding. Use of new fillers and welding technologies enables successfully joining advanced structural materials with special properties such as those of intermetallics of Ni–Al and Ti–Al systems, high-strength quasicrystalline aluminium alloys, nanodispersed or nanolayered light composite materials.

Diffusion welding allows joining predominantly compact small-sized products and components for aircraft and rocket engines, and is also applied in manufacturing of equipment for nuclear engineering, electrical and electronic engineering.

Friction stir welding is used in manufacture of products of large dimensions and diverse shape, for instance, flat panels and shells, panels and volume frames, tanks for liquid fuel and cases of various machines. Butt, fillet or overlap welds (straight and curvilinear, extended, intermittent and spot) are made [5].

The authors are expressing their sincere gratitude for active participation in performance of this research to Yu.V. Milman, Corresp. Member of NASU,

A.I. Sirko and L.A. Olikhovsky, Cand. of Sci. (Eng.), G.K. Kharchenko, Dr. of Sci. (Eng.), Yu.V. Falchenko and A.G. Poklyatsky, Cand. of Sci. (Eng.), V.E. Fedorchuk, A.N. Muravejnik, Yu.A. Khokhlova, A.A. Chajka, Eng.

1. Movchan, B.A. (2004) Electron beam technology of vapor phase evaporation and deposition of inorganic materials with amorphous, nano- and microdimensional structure. *Nanosistemy, Nanomaterialy, Nanotekhnologii*, 2(**4**), 1103–1126.
2. Inoue, A., Kimura, H. (2000) High-strength aluminum alloys containing nanoquasicrystalline particles. *Mater. Sci. and Eng. A*, 286(**1**), 1–10.
3. Ustinov, F.I., Olikhovskaya, L.A., Polishchuk, S.S. (2006) Metastable nanostructural states in coatings of Ni–Al system made by vapor phase deposition. *Metallofizika i Nov. Tekhnologii*, **6**, 32–37.
4. Ryabov, V.R., Muravejnik, A.N., Bondarev, A.A. et al. (1999) Study of structure of welded joints of dispersion-strengthened aluminium alloy. *Tekhnologiya Lyog. Splavov*, **1 / 2**, 139–144.
5. Ishchenko, A.Ya., Podielnikov, S.V., Poklyatsky, A.G. (2007) Friction stir welding of aluminium alloys (Review). *The Paton Welding J.*, **11**, 25–30.
6. Milman, Yu.V. (2005) Mechanical behavior of nanostructured aluminium alloys containing quasicrystalline phase. *Mater. Sci. Forum*, **482**, 77–82.
7. Ishchenko, A.Ya., Tretyak, N.G., Lozovskaya, A.V. et al. (1993) Weldability of nanodispersed material of Al–Al_2O_3 system produced by vapor phase condensation. *Avtomatich. Svarka*, **5**, 16–19.
8. Ishchenko, A.Ya., Kharchenko, G.K., Falchenko, Yu.V. et al. (2006) Vacuum solid-phase joint of dispersion-strengthened composite materials. *Nanosistemy, Nanomaterialy, Nanotekhnologii*, 4(**3**), 747–756.
9. Ishchenko, A.Ya., Falchenko, Yu.V., Ustinov, A.I. et al. (2007) Diffusion welding of finely-dispersed AMg5 / 27 % Al_2O_3 composite with application of nanolayered Ni / Al foil. *The Paton Welding J.*, **7**, 2–5.
10. Povarova, K.B., Bannykh, O.A. (1999) Principles of producing of intermetallic-base structural alloys. Part 1. *Materialovedenie*, **2**, 27–33; Part 2. *Ibid.*, **3**, 29–37.
11. Yushtin, A.N., Zamkov, V.N., Sabokar, V.K. et al. (2001) Pressure welding of intermetallic alloy γ-TiAl. *The Paton Welding J.*, **1**, 33–37.
12. Duarte, L.I., Ramus, A.S., Vieira, M.F. et al. (2006) Solid-state diffusion bonding of gamma-TiAl alloys using Ti / Al thin films as interlayers. *Intermetallics*, **14**, 1151–1156.
13. Ustinov, A.I., Falchenko, Yu.V., Ishchenko, A.Ya. et al. (2008) Diffusion welding of gamma-TiAl based alloys through nanolayered foil of Ti / Al system. *Ibid.*, **16**, 1043–1045.
14. Milman, Yu.V., Sirko, A.I., Iefimov, M.O. et al. (2006) High strength aluminium alloys reinforced by nanosize quasicrystalline particles for elevated temperature application. *High Temperature Materials and Processes*, 25(**12**), 19–29.
15. Poklyatsky, A.G., Ishchenko, A.Ya., Yavorskaya, M.R. (2007) Strength of joints on sheet aluminium alloys produced by friction stir welding. *The Paton Welding J.*, **9**, 42–45.

STABILISATION OF ELECTRODE MELTING RATE IN ROBOTIC ARC WELDING

G.A. TSYBULKIN
E.O. Paton Electric Welding Institute, NASU, Kiev, Ukraine

One of the approaches to reduction of external disturbances affecting the electrode melting rate in robotic arc welding is considered. The procedure providing synthesis of the compensating circuit, based on the invariance principle, is described. Computer simulation results are presented.

Keywords: arc welding, robotics, stabilisation of conditions, compensation of disturbances, structural synthesis

It is a well known fact that the key destabilising factors in automatic metal arc welding are unpredictable changes in: a) voltage at output terminals of the welding current source; b) electrode wire feed speed; and c) distance between the tip of the current-conducting nozzle and free surface of the weld pool. The issues of decreasing the effect of these factors on quality of the welded joints are described in numerous studies, which suggest a number of interesting approaches [1–8]. The idea they share consists in stabilisation of the arc welding process parameters in one way or another. Study [7] puts forward cross-connections between the welding current source voltage and electrode wire feed speed to provide partial stabilisation of the above parameters. Study [8] proposes using the absorption principle to achieve a more substantial decrease in the effect of the destabilising factors. This principle is based on compensation of external disturbances through adding a specially synthesised compensation connection to a structural scheme of the welding circuit.

Meanwhile, robotic arc welding is characterised by the feasibility of compensating for the harmful effect of the destabilising factors with no structural changes in the welding circuit proper. In particular, the fluctuations of voltage that form at the output terminals of the welding current source can be compensated for in some cases by means of corrective control of distance between the tip of the torch located in a gripping device of the industrial robot and free surface of the weld pool as function of the above voltage.

The present study considers the problem of synthesis of structure of the compensating circuit and algorithm of the corrective control of position of the welding torch using a manipulation robot on the basis of current information on a change in voltage of the welding current source.

Consider a mathematical model of the welding circuit in the form of a structural scheme (Figure 1) by using the following designations: v_e — metal electrode feed speed with respect to the torch nozzle; v_m — electrode melting rate; $\Delta v = v_e - v_m$; H — distance between the tip of the current-conducting nozzle and free surface of the weld pool; h — electrode extension; l — length of the arc gap; $E \equiv du_a / dl$ — intensity of the electric field in the arc column; u_a — arc voltage; u_0 — sum of the near-electrode voltage drops; u_s — voltage at the output terminals of the welding current source; $\Delta u = u_s - u_a - u_0$; $M \equiv dv_m / d_i$ — steepness of the electrode melting characteristic at rated values i_{rated} of the welding current and electrode extension h_{rated}; $R_* = R + S_a - S_s$, where R is the total resistance of lead wires, electrode extension and sliding contact in the torch nozzle; $S_a \equiv du_a / d_i$; $S_s \equiv du_s / d_i$ — steepness of volt-ampere characteristics of the arc and welding current source at rated value i_{rated} of the current; L — inductance of the welding circuit; and $D = d / dt$ — operator of differentiation.

According to the structural scheme shown in Figure 1, write down equation of the electrode melting rate in the operator form:

$$v_m = W\left(v_e - DH + \frac{1}{E}\,Du_s\right), \qquad (1)$$

where

$$W = W(D) = \frac{1}{T_e T_s D^2 + T_s D + 1};\quad T_e = \frac{L}{R_*};\quad T_s = \frac{R_*}{EM}.$$

It can be seen from expression (1) and Figure 1 that the external disturbances affecting speed v_e, distance H and voltage u_s may lead to deviation of electrode melting rate v_m from its rated values, which, naturally, may impact quality of the welded joint. In robotic arc welding, the fluctuations of electrode wire feed speed v_e are insignificant, as a rule. Unpredictable changes in voltage u_s at the output terminals of the welding current source are most often related to load instability in the industrial mains. In this connection, consider a case where v_e = const, and disturbance of the rated arc welding conditions is caused by a short-time change in voltage u_s.

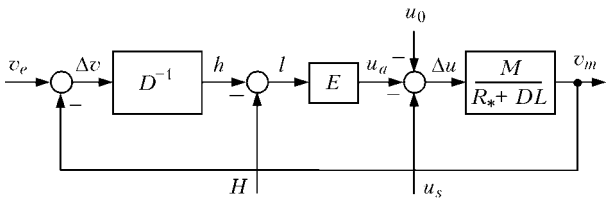

Figure 1. Structural scheme of welding circuit (for designations see the text)

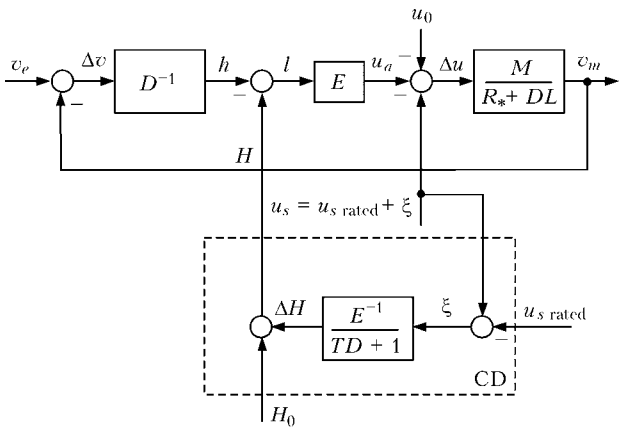

Figure 2. Structural scheme of compensation circuit

It can be easily seen from analysis of expression (1) that to ensure independence of electrode melting rate v_m upon fluctuations of u_s it is enough to meet the following condition:

$$\frac{1}{E} Du_s - DH = 0, \tag{2}$$

which, according to the theory of automatic control [9–12], can be called the invariance condition with respect to disturbances. It is known that the main problem of the invariance theory is to find such structural solutions, at which arbitrary-type external disturbances could have a minimal negative effect on behaviour of a controlled process. The most favourable situation for solving this problem is when it is possible to directly measure the external disturbances, although the laws of their changes with time may not be known beforehand. In our case, any deviations in $\xi(t) = u_s(t) - u_{s\,\text{rated}}$, where $u_{s\,\text{rated}}$ is the rated value of voltage of the welding current source, can be readily measured. Therefore, to meet condition (2) it is sufficient to ensure the automatic control of distance H in accordance with the algorithm:

$$H(t) = H_{\text{rated}} + \Delta H(t), \tag{3}$$

where

$$\Delta H(t) = \frac{1}{E} \xi(t). \tag{4}$$

It is clear that algorithms (3) and (4) in the above form are physically unrealisable, as the actuators, whose task is to provide spatial movement of the welding torch, have some lag effect. Therefore, let us modify expression (4) as follows by using the mathematical model of an inertial link:

$$\Delta H(t) = \frac{1}{E(TD + 1)} \xi(t), \tag{5}$$

where T is the time constant of the actuators.

Structure of the compensating circuit based on algorithms (3 and (5) is shown in Figure 2. It can be seen from this Figure that the requirement to structure of the circuit, formulated as the two-channel principle [10], is met: disturbance $\xi(t)$ is transmitted via two channels, and the total effect at exit of these channels is $\sigma = \Delta u - \Delta u_* = \xi TD / (TD + 1)$, where $\Delta u_* = \Delta u$ at $\xi = 0$ is much lower than $\xi(t)$ at low T. Hence, electrode melting rate v_m becomes invariant to some extent with respect to disturbing effect $\xi(t)$.

Characteristic peculiarity of this method for compensation of disturbances is that the compensation device (CD) (Figure 2), which in fact is an external device with respect to the welding circuit, does not introduce any changes into its structure, in contrast to other known methods. The $\xi(t)$ signal read out from the sensor of voltage u_s arrives, after preliminary processing, directly to the control device of the manipulation robot, which, according to algorithm (5), moves the welding torch to calculated distance $\Delta H(t)$,

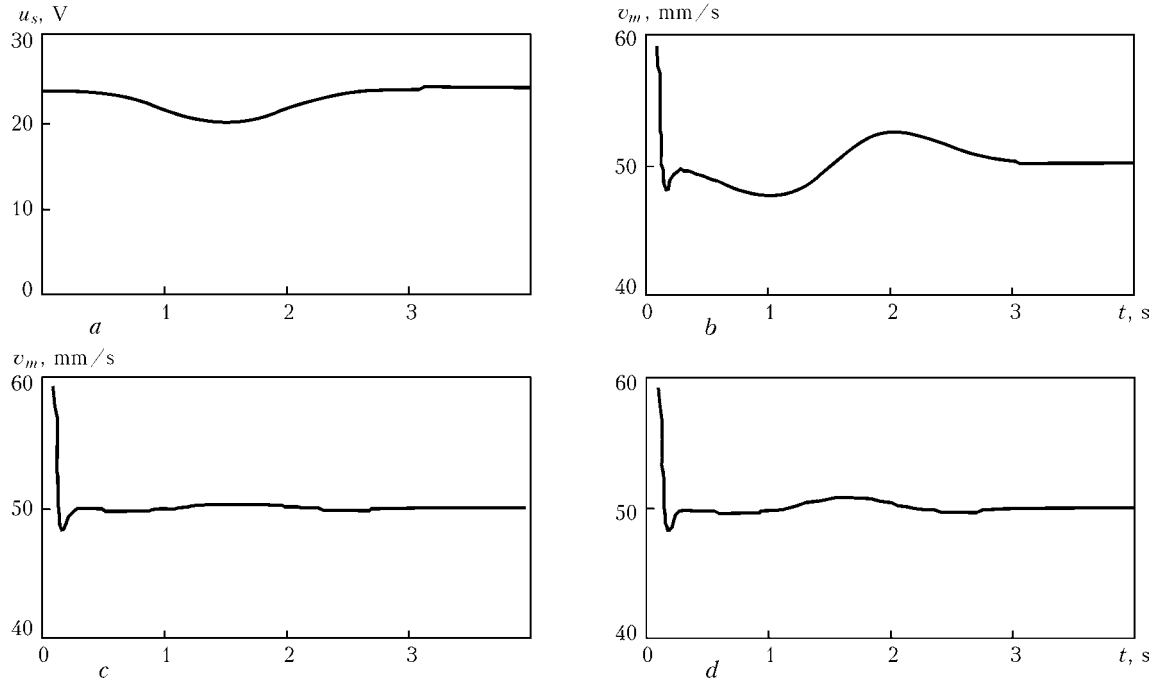

Figure 3. Results of computer simulation (see explanations in the text)

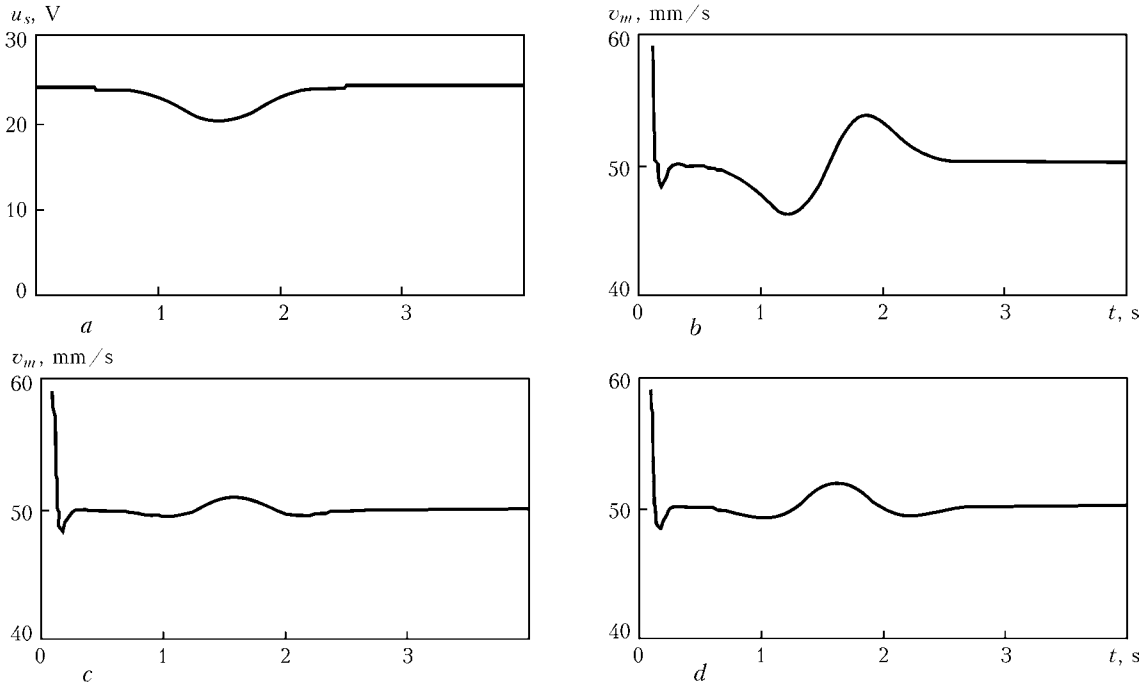

Figure 4. Results of computer simulation (see explanations in the text)

thus decreasing the effect of disturbance $\xi(t)$ on electrode melting rate $v_m(t)$.

Computer simulation of dynamics of the processes occurring in the circuit during arc welding was carried out to experimentally check the efficiency of the suggested approach to stabilisation of electrode melting rate v_m. Numerical values of parameters of the circuit and arc welding process were as follows: $L = 7 \cdot 10^{-4}$ H; $R = 0.015$ Ohm; $S_a = 0.005$ V / A; $S_s = -0.02$ V / A; $u_s = 24$ V; $u_0 = 12$ V; $v_e = 50$ mm / s; $H = 17$ mm; $E = 2$ V / mm; and $M = 0.38$ mm / (A·s).

Variation in voltage u_s at the output terminals of the welding current source was regarded as an external disturbance, the law of changes of which was set by the following relationship:

$$u_s(t) = 24 - \xi(t), \qquad (6)$$

where

$$\xi(t) = 4 \exp [- n(t - 1.5)^2]. \qquad (7)$$

(Graphs of function (6) at $n = 2$ s^{-2} and $n = 5$ s^{-2} are shown in Figures 3, *a*, and 4, *a*, respectively.)

Results of simulation of process (1) at the disturbances of type (7) are presented in Figures 3 and 4, which show graphs of changes of $v_m(t)$ in the welding current without CD (Figure 3, *b*, and Figure 4, *b*) and with CD (Figure 3, *c*, *d*, and Figure 4, *c*, *d*). It can be seen by from these graphs that at the absence of CD (see Figure 1) disturbance (7) leads to a substantial change in electrode melting rate $v_m(t)$ (Figure 3, *b*, and Figure 4, *b*). Upon connecting CD (see Figure 2), the effect of disturbance (7) on electrode melting rate $v_m(t)$ becomes much mitigated (Figure 3, *c*, *d*, and Figure 4, *c*, *d*).

As might be expected, the extent of compensation of disturbance $\xi(t)$ in the given scheme depends upon the lag effect of the actuators that move the torch. Figure 3, *d* shows graph $v_m(t)$ plotted for $T = 0.05$ s, and Figure 4, *d* — for $T = 0.1$ s. It can be seen from these graphs that the extent of compensation of disturbances grows with decrease in the lag effect of the actuators.

It can be well seen by comparing graphs in Figure 3, *c*, *d*, and Figure 4, *c*, *d* that the «slower» disturbances affect electrode melting rate v_m to a lesser degree than the «rapid» ones. This shows that the disturbances the speed of changes of which is lower than the speed of attenuation of the transient processes are compensated for most efficiently in the welding circuit.

Therefore, as shown by the results of computer simulation, adding an extra connection between the welding current source and torch movement control device to the system of robotic control of the metal arc welding process can be a very efficient method for compensation of slow fluctuations in voltage of this source.

1. Paton, B.E. (1958) Some problems in the field of automatic control of welding processes. *Avtomatich. Svarka*, **4**, 3–9.
2. Paton, B.E., Lebedev, V.K. (1966) *Electric equipment for arc and slag welding*. Moscow: Mashinostroenie.
3. Dyurgerov, N.G., Penivshi, V.A., Sagirov, Kh.N. (1966) About stability of metal-electrode pulse-arc welding process. *Svarochn. Proizvodstvo*, **7**, 13–14.
4. Gladkov, E.A. (1976) *Automation of welding processes*. Moscow: N.E. Bauman MVTU.
5. Lebedev, A.V. (1978) Efficiency of stabilisation of mean value of the current in semiautomatic welding. *Avtomatich. Svarka*, **10**, 37–41.
6. (1986) *Automation of welding processes*. Ed. by V.K. Lebedev, V.P. Chernysh. Kiev: Vyshcha Shkola.
7. Paton, B.E., Shejko, P.P., Zhernosekov, A.M. et al. (2003) Stabilization of the process of consumable electrode pulse-arc welding. *The Paton Welding J.*, **8**, 2–5.
8. Tsybulkin, G.A. (2007) Compensation of external disturbance action on consumable electrode arc welding mode. *Ibid.*, **4**, 5–8.
9. (1987) *Reference book on automatic control theory*. Ed. by A.A. Krasovsky. Moscow: Nauka.
10. Tsybulkin, G.A. (1979) Invariance and stability of one class of combined software systems with variable scale of program time. In: *Theory of invariance and its application*. Pt 2. Kiev: Naukova Dumka.
11. Kukhtenko, A.I. (1963) *Problems of invariance in automation*. Kiev: Gostekhizdat Ukr. SSR.
12. Tsypkin, Ya.Z. (1996) Synthesis of structure of stabilising and invariant regulators. *Doklady RAN*, 347(**5**), 607–609.

SYSTEM FOR TIG WELDING PROCESS CONTROL OF LOW-THICKNESS STEELS

D.D. KUNKIN
E.O. Paton Electric Welding Institute, NASU, Kiev, Ukraine

The version of the pulsed-arc welding mode using a low-amperage welding current source with the PWM regulation and an experimental control system with application of microprocessor devices is presented.

Keywords: TIG welding, pulsed arc, microprocessor, regulation using pulse-width modulation, thin-sheet metal

The TIG welding of steels up to 0.5 mm thickness is widely used in instrument making (assembly of housings and screens) and to a smaller degree in automotive industry in performance of repair-restoration works. Other fields of its narrowly specialized application are possible as well where use of standard welding invertors is inadvisable.

In this work the issue was solved to build a control system for welding of a thin-sheet metal with the least material expenses and consumption of time. For reducing heat input into the metal and probability of burn-through the direct current welding with low- and medium-frequency modulation (pulsed-arc welding) was used. Regulation of the current duration in the pulse and in the pause, and frequency of repetition of the pulses was performed using the ATMEGA8515 microcontroller (of the Atmel company). In the modulated current welding by means of changing of minimum four regulated parameters (pulse duration, frequency of its repetition, current amplitude in the pulse, and the base current level) it is possible to establish optimal conditions for welding. On the experimental specimen it is convenient to use a unified programmable module for processing commands of a welder and controlling regulated parameters with indication of the set values, which allows adopting the control system according to different requirements and tasks [1, 2].

As object of the control a low-amperage welding current source was used, developed at the sub-unit of the E.O. Paton EWI ---- State Scientific-Engineering Center of Welding and Control in the Field of Nuclear Power Engineering of Ukraine. This source of current is a component of the simulator for a welder (Figure 1) and represents a pulse-width down-converter with the control system.

Stabilization of the welding current using the feedback signals, received from the current sensor *3*, is performed according to the law of the pulse-width modulation, implemented by the TL 494 microcircuit *1*. For matching output signal of the microcircuit *1* and the power transistor the IR 2110 microcircuit-driver *2* is used. The current feedback signal from the sensor is compared with the reference voltage level, due to which signal of the error is produced that is compared with the saw-tooth signal. As a result the power transistor control pulses are formed with a frequency which is determined by parameters of the external time-setting circuit of the saw-tooth voltage generator (STVG), in our case it equaled 20 kHz. Duration of open state of the transistor is directly proportional to difference between the error signal and the reference voltage. Due to stored energy of the choke L1 the current pulses transform into continuous current, mean value of which is maintained at constant level with a certain accuracy.

Conditions of the pulsed-arc welding were implemented as follows. The microcontroller ensures generation of the signal, time diagram of which is presented in Figure 2. In the program adjustment by the operator of the pulse cycle duration and the pause directly in the course of the device operation with 50 μs discreteness is foreseen. A welder using the keys «higher» / «lower» (or digital potentiometers) sets values of the coefficients which correspond to the duration of the pulse T_{pulse} and the pause T_{pause} (from 0 to 225) which are multiplied by 50 μs. Frequency of the output pulses may be determined using the formula

$$f_{out} = 1 / (T_{pulse}T + T_{pause} + dt) \text{ [Hz]},$$

where dt is the «dead time» duration (duration of the control resistor switched-off state before each new cycle) equal to 10 μs; T is the program time unit equal to 50 μs.

Pulsed signal of the assigned frequency is fed from the microcontroller *6* to the optron key *5*. The key shunts the reference voltage attenuator resistor *4*, the compared level of the reference voltage sharply increases, due to which open state of the power transistor increases, and value of the welding current approaches the maximum one. Ratio between maximum and minimum values of the current may be changed by the operator. Frequency of the jump-like change of the reference signal is determined by frequency of the microcontroller pulse generation and is selected by the operator as combination of the pulse and the pause duration. Its selected values are imaged on the seven-segment indicator of the dynamic indication unit *7*.

Maximum frequency of the output signal, which is the modulation frequency, equals f_{out} =

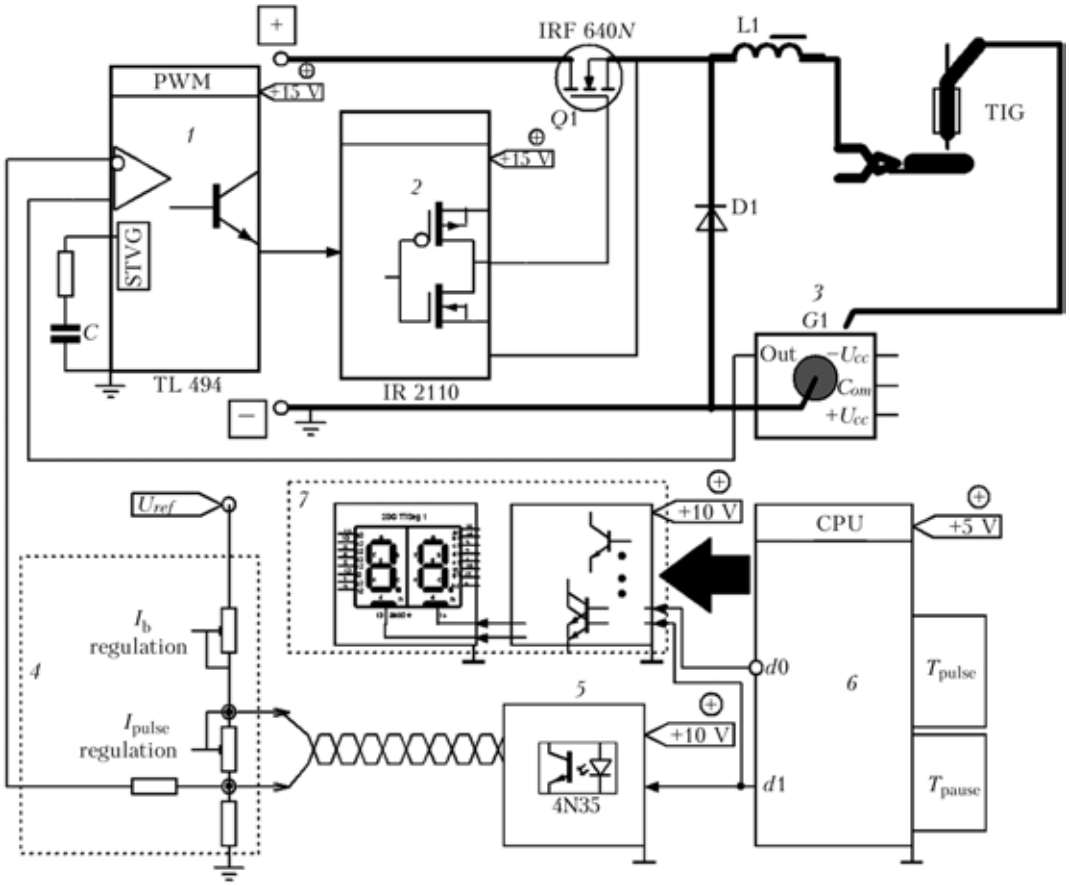

Figure 1. Structural scheme of device for pulsed-arc welding

$= 1 \cdot 10^6 / (1 \cdot 50 + 1 \cdot 50 + 10) = 9.1$ kHz. It should be noted that such f_{out} value of the welding current enables increase of the arcing stability but does not effect its energy parameters because of inertia of the heat processes. Minimum value of the output signal frequency equals 39.2 Hz.

In the course of carrying out the experiments acceptable stability of the arcing without burns-through was achieved at the following parameters of the process: steel –– the galvanized ST0 sheet of 0.55 mm thickness; duration of the pulse and the pause was 4.9 ms ($T_{pause} = T_{pulse} = 98$) which corresponds to the frequency of pulses $f_{out} = 100$ Hz at relative pulse duration of 50 %. Range of the jump-like change of the reference voltage constitutes 50 % of the base value. So, for maximum current (10 A) the range of its pulsations equals approximately 5 A, whereby voltage values in the arc gap vary from 16 to 20 V. Oscillogram of the modulated welding current is presented in Figure 3.

Proceeding from results of the carried out work one may draw the following conclusions.

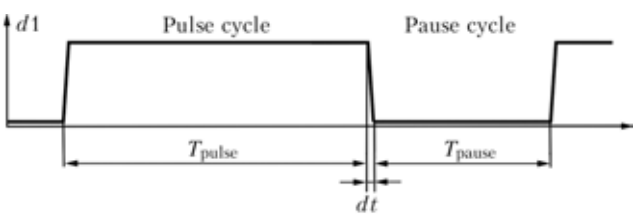

Figure 2. Control signal of microcontroller

Described method of building the control system for pulsed-arc welding of a thin-sheet metal is economical and at the same time sufficiently flexible solution for different fields of application. Shortcoming of such method for achieving welding current pulsations consists in periodic change of amplification factor of the error signal amplifier due to which accuracy of the current stabilization in the pulse is worse than in the pause. Adjustment of the pulse and the pause current levels does not occur independently, it is performed simultaneously, due to which the operator needs long time to perform adjustment of the necessary current values. The advantage consists in convenience of digital independent regulation of the pause pulse duration. If it is necessary to significantly change frequency range of the welding current (in direction of the frequency reduction), there is not need to replace discrete elements of the control system. Range of the

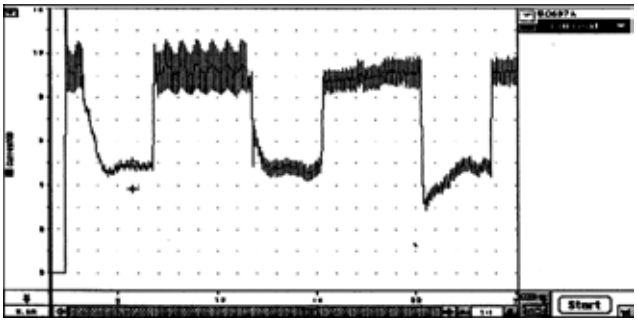

Figure 3. Modulated current for pulsed-arc welding (2 A –– 5 ms scale)

pulse and the pause duration regulation changes depending upon the program time unit.

In future it will be advisable to single out from the data array, obtained during performance of experiments in welding of metals of various thicknesses, optimal ranges of regulation of main parameters of the welding current for achieving established minimum influence of temperature, depth of penetration, and stability of the welding process. Presented control scheme may be used with certain amendments for a similar welding current source of 4 kW power.

1. Baranov, V.N. (2004) *Application of AVR microcontrollers: schemes, algorithms*. Moscow: Dodeka-XXI.
2. Trampert, V. (2007) *Measurement, control and regulation using AVR microcontrollers*. Kiev: MK-Press.

MECHANISM OF THE EFFECT OF SCANDIUM ON STRUCTURE AND MECHANICAL PROPERTIES OF HAZ OF THE ARC WELDED JOINTS ON ALUMINIUM ALLOY V96

Yu.A. KHOKHLOVA, A.A. CHAJKA and **V.E. FEDORCHUK**
E.O. Paton Electric Welding Institute, NASU, Kiev, Ukraine

Heating of base metal in arc welding of high aluminium alloy V96 leads to melting of low-melting point (eutectic) phases along the grain boundaries in HAZ. These phases are the cause of hot cracking of HAZ, while after cooling they decrease the level of mechanical properties of the joints. Scandium additions to the alloy slow down recrystallisation processes, thus promoting formation of a dispersed structure of the eutectic precipitates along the grain boundaries and, consequently, improvement of mechanical properties of the joints.

Keywords: aluminium alloys, arc welding, hot shortness, structural transformations, eutectic, scandium, strength, micromechanical tests, Berkovich indenter, microhardness, Young modulus, ductility coefficient

Heating of base metal in arc welding of high alloy V96 leads to melting of low-melting point components to form brittle interlayers in the fusion zone after cooling, thus causing initiation of solidification cracks [1] (Figures 1, 2). Alloys of this type are categorised as the strongest aluminium alloys. They are intended for production of light extruded and forged parts in machine building, and used as experimental structural materials [2]. Scandium, which is an expensive material, is usually added to alloy V96 to prevent initiation of solidification cracks. Scandium additions are known to have a positive effect on mechanical properties of aluminium alloys, which shows up in modification of cast structure, increase in recrystallisation temperature, as well as precipitation hardening and structural strengthening.

The effect of scandium on many advanced aluminium alloys has been well studied up to now [3], and many scandium-containing aluminium alloys are available. However, the effect of scandium on the processes occurring in HAZ and weld metal remains little investigated as yet.

The purpose of this study was to investigate the mechanism of the effect of scandium on improvement of structure and micromechanical properties of the eutectic formed along the fusion boundary in HAZ during arc welding.

The procedure used to conduct a set of mechanical investigations provides for making of simulation specimens of the alloys, whose chemical and structural

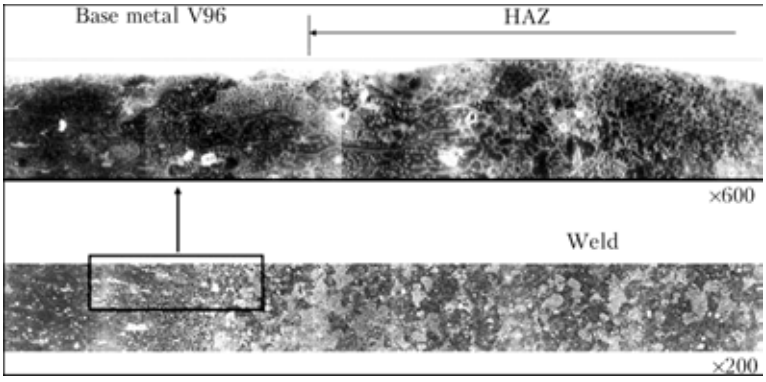

Figure 1. Microstructure near HAZ of the arc welded joint on alloy V96

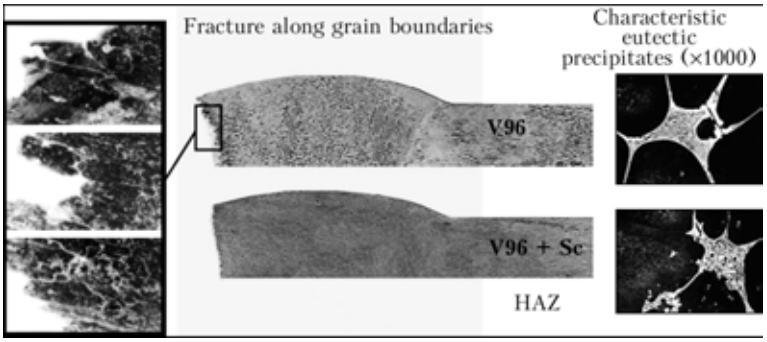

Figure 2. Microstructure of fracture along the grain boundaries at the sites of concentration of brittle interlayers of low-melting point components (×800) and near HAZ (×1200) of the arc welded joints on alloys V96 and V96 + Sc

Chemical composition (wt.%) of initial alloys V96 and V96 + Sc*

Alloy	Zn	Mg	Cu	Sc	Mn	Zr
V96	8.4–8.8	2.5--2.7	2.4–2.6	–	0.20–0.26	0.15--0.18
V96 + Sc	8.6–8.9	2.6--2.8	2.1–2.4	0.27–0.31	0.19–0.25	0.15--0.18

*Balance ---- aluminium.

composition corresponds to that of the eutectic of brittle interlayers formed within the fusion zone of the welds. Arc welded joints of two modifications of the V96 type alloy were used as a material for the investigations. Chemical composition of initial alloys V96 and V96 + Sc is given in the Table and shown in a section of the 460° isothermal tetrahedron of the Al–Mg–Cu–Zn system (8 wt.% Zn), comprising the following phases (Figure 3) [4, 5]: α ---- Mg, Zn, Cu solid solution in Al; θ ---- $CuAl_2$; *S* ---- Al_2CuMg; *T* ---- AlCuMgZn (forms $Al_2Mg_3Zn_3$ and Al_6CuMg_4 phases); *M* ---- AlCuMgZn (forms phases $MgZn_2$ of the Mg–Zn system and AlCuMg of the Al–Cu–Mg system); *Z* ---- AlCuMgZn (forms phases Mg_2Zn_{11} of the Mg–Zn system and $Al_{10}Cu_7Mg_3$ of the Al–Cu–Mg system).

Scandium is characterised by low (0.35 %) solubility in solid aluminium. Primary intermetallics emerge as early as at its concentration that is a bit higher than the limiting one. They form under conventional casting conditions and have the form of coarse, non-uniformly distributed inclusions [6].

The process of melting and solidification of both alloys occurs in two stages. First the low-melting point eutectic melts at a temperature of 480 °C. This short-time process ends quickly, and melting of the solid solution occurs starting from 580 °C. In cooling, first the solid solution and then eutectic solidify [7]. The entire solidification range is approximately 170 °C, the portion of the eutectic solidification range being insignificant (less than 2 %). The data obtained on formation of the eutectic in a wide temperature range of 480–580 °C are indicative of the probability of occurrence of the eutectic precipitates and embrittlement of the HAZ metal at a considerable distance from the fusion boundary, while those on a wide range of solidification of the alloy and low content of the eutectic at the final stage of solidification are indicative of an increased sensitivity to hot cracking in the weld metal.

Fine structure of the weld metal, characterised by the presence of continuous eutectic precipitates along the boundaries and cells of dendrites, is formed in

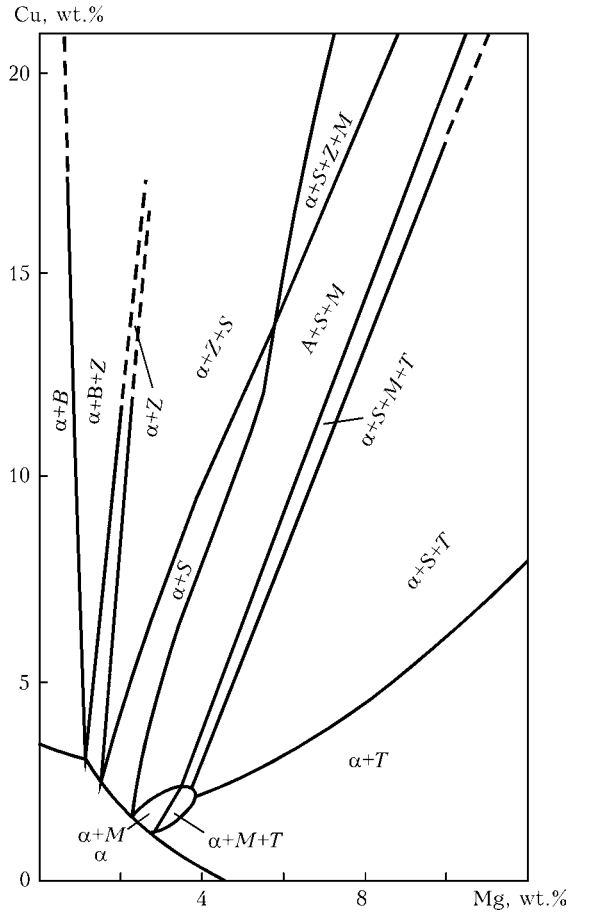

Figure 3. Section of isothermal tetrahedron 460° of Al–Mg–Cu–Zn system (8 wt.% Zn)

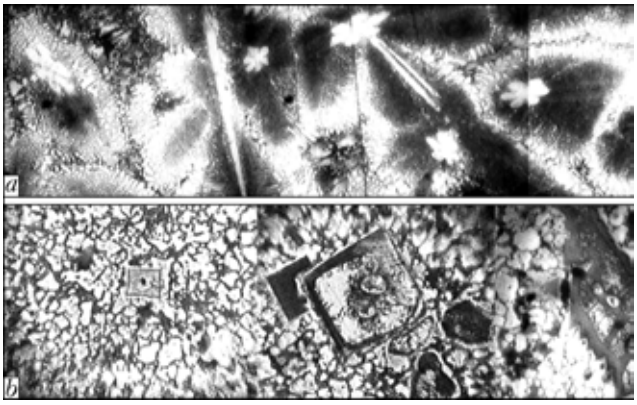

Figure 4. Microstructure of eutectic in simulation specimens of arc welded joints on alloys V96 (*a*) and V96 + Sc (*b*) (×600)

welding of alloy V96. Addition of scandium to the alloy leads to refining of grains, formation of a sub-dendrite structure, and change in the character of distribution of the eutectic. Grain size in the weld metal containing 0.3 % Sc decreases from 0.100–0.500 to 0.030–0.001 mm. The eutectic precipitates are located only along the sub-dendrite grain boundaries (see Figure 1). Isolated intermetallics of a regular geometric shape, 3–7 μm in size, form in the weld metal on alloy V96 + Sc.

Examination of structure of the HAZ region at a liquid–solidus temperature revealed different eutectic formations in both alloys. Their shape and size are affected by the initial structure of the base metal. For example, in the case of continuous stringer-type precipitates of the redundant phases the eutectic precipitates are thin and extended, whereas at the presence of isolated inclusions they form local eutectic volumes. The latter are concentrated in locations of the redundant phases. With distance to the fusion boundary and increase in temperature, first the high-angle grain junctions melt to form continuous interlayers. With an addition of scandium to the base metal, the melting process becomes less reactive. It is mostly of a local character (except for extended eutectic structure formations), and decrease in the recrystallisation extent takes place. Inclusions of the aluminium-scandium phases persist in HAZ in a somewhat modified form. They are distributed both in the bulk of grains and in the eutectic clusters.

Chemical composition of the eutectic precipitates along the grain boundaries was determined by the method of X-ray microanalysis of HAZ of the joints on alloys V96 and V96 + Sc made by arc welding using no filler wire.

Eutectic precipitates in alloy V96 had the following chemical composition, wt.%: 28 Zn, 15.9 Cu, 10.5–11.0 Mg (compact eutectic inclusions), and 27.7 Zn, 16 Cu, 12.0–12.5 Mg (continuous boundary inclusions), i.e. the eutectics had an almost identical compositions independently of their form. Eutectic precipitates in alloy V96 + Sc were characterised by a wide range of changes in the content of elements. Detailed X-ray microanalysis of different points of the precipitates made it possible to detect two types of the eutectics. The first was characterised by an increased content of the following elements, wt.%:

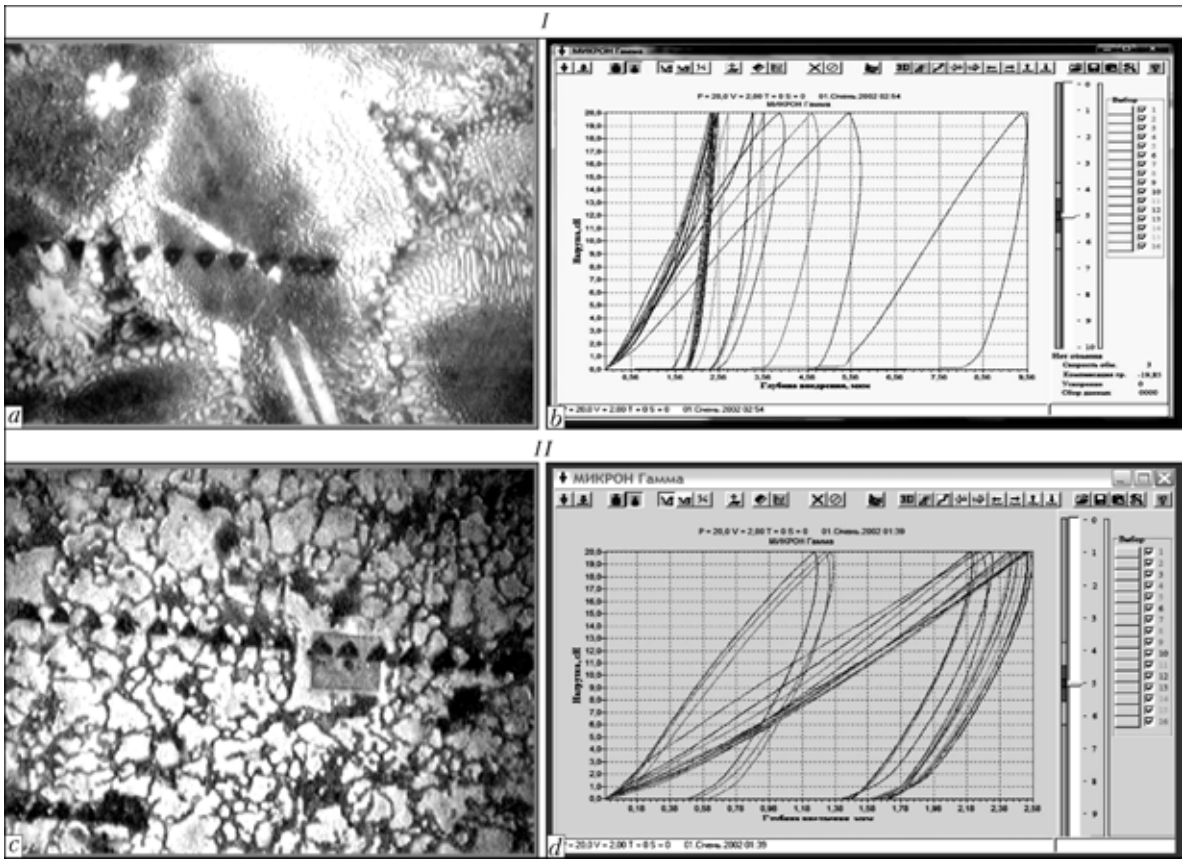

Figure 5. Indentations (*a*, *c* — ×600) and loading-unloading diagram (*b*, *d*) for eutectics of alloys V96 (*I*) and V96 + Sc (*II*)

25–27 Zn, 17.9–18.2 Cu and 11.7–12.0 Mg; and the other ---- by their decreased content (15.5–18.2 Zn, 8–21 Cu and 4.6–5.3 Mg) and presence of 3.1–8.4 Sc.

Ingots that simulated structure and chemical composition of the eutectic of melted interlayers near the fusion boundary in arc welding were melted. The ingots of the required chemical composition were produced from the alloys containing the following elements, wt.%: 28 Zn, 16 Cu, 13 Mg, balance ---- aluminium, and 17 Zn, 10 Cu, 5 Mg, 6 Sc, balance ---- aluminium. The use was made of electrolytic copper and zinc, and high-purity aluminium A995. Scandium was added from the master alloy containing 2 wt.% Sc, which was preliminarily melted in a crucible and then gradually cooled to room temperature. Intermetallic inclusions settled on the mould bottom to form the ingot layer containing 16 % Sc. According to the data of X-ray microanalysis, the distribution of scandium in height of an ingot was as follows, wt.%: 16.600 in the lower part, 0.511 in the middle, and 0.470 in the upper part. Scandium was added to the charge from the lower layer of the ingot. Melting was performed in a graphite crucible of the muffle furnace. Molten metal was cast into a special shape, which made it possible to immediately produce specimens of the MI-3 type for mechanical tests and examination of their structure and chemical composition.

As shown by metallographic examinations, cast specimens had primarily the eutectic structure. The specimens that corresponded to the Al–Zn–Cu–Mg alloy eutectic had a more non-uniform and coarse-dendrite structure (Figure 4, *a*). The scandium-containing eutectic was more dispersed. However, it contained isolated coarse scandium intermetallics (Figure 4, *b*).

Mechanical properties of the alloys corresponding to eutectics Al–Zn–Mg–Cu and Al–Zn–Mg–Cu–Sc were determined on the specimens of the above type, which fractured by the brittle mechanism without formation of the plasticity regions. The character of fracture changed from that of a deep penetration to the straight-lined one, the eutectic having an increased strength value (in the presence of scandium). Strength of the specimens of alloy V96 + Sc was 141 MPa, and that of alloy V96 ---- 134 MPa.

Micromechanical tests were carried out with the «Micron-Gamma» computerised probe system using the Berkovich trihedral indenter [8, 9]. Microhardness of the eutectic of alloy V96 of a different shape and etching ranged from 0.024 to 0.390 GPa. Light eutectic had the maximal value of microhardness, and the minimal value of microhardness was detected in the middle of dark coarse secondary dendritic structures (Figure 5, *a*). Microhardness of alloy V96 + Sc was 0.325–1.324 GPa, and that of the dark phase was 1.324 GPa. Microhardness of isolated coarse scandium intermetallics differed but insignificantly from that of the scandium-containing eutectic (Figure 5, *b*), the values of Young modulus being 40 % higher compared with the scandium-containing eutectic. The values of microhardness of the eutectic of alloy V96 + Sc were 41 % higher than those of alloy V96. The ductility coefficient of the eutectics remained at the same level.

Therefore, embrittlement in welding of alloy V96 occurs at a substantial distance from the fusion boundary. Scandium additions to alloy V96 slow down the recrystallisation processes and decrease the liquation level. Modification of the alloy leads to improvement of its structure and preservation of ductility, and provides increase of 41 % in microhardness, 40 % in Young modulus, and 5 % in strength.

1. Ovsyannikov, B.V., Doroshenko, N.M., Zamyatin, V.M. (2005) Solidification cracks in ingots of high-strength aluminium alloys. *Tekhnologiya Lyog. Splavov*, **1–4**, 117–121.
2. Fridlyander, I.N. (2002) Aluminium alloys in aircraft of the 1970–1999 and 2000–2015 periods. *Ibid.*, **4**, 12–17.
3. Fridlyander, I.N., Chuistov, K.V., Berezina, A.L. et al. (1992) *Aluminium-lithium alloys. Structure and properties*. Kiev: Naukova Dumka.
4. Mondolfo, L.F. (1979) *Structure and properties of aluminium alloys*. Moscow: Metallurgiya.
5. (1977) *Constitutional diagrams of aluminium- and magnesium-base systems*: Refer. Book. Moscow: Nauka.
6. Volkov, V.A. (1987) *Effect of alloying elements on the processes of decomposition of Al–Li and Al–Sc alloys*: Syn. of Thesis for Cand. of PhM Sci. Degree. Kiev.
7. Berezina, A.L., Volkov, V.A., Domashnikova, B.P. et al. (1987) Some peculiarities of decomposition of oversaturated solid solution of Al–Sc system alloys. *Metallofizika*, 9(**5**), 43–45.
8. Grigorovich, V.K. (1976) *Hardness and microhardness of metals*. Moscow: Nauka.
9. Oliver, W.C., Pharr, G.M. (2004) Measurement of hardness and elastic modulus by instrumented indentation: advances in understanding and refinements to methodology. *J. Mater. Res.*, **19**, 3–20.

LASER-ASSISTED HARDENING AND COATING PROCESSES (REVIEW)

V.Yu. KHASKIN
E.O. Paton Electric Welding Institute, NASU, Kiev, Ukraine

The paper considers the state-of-the-art in the field of heat hardening, alloying, cladding and coating processes, in which the main role is given to laser radiation. Flow diagrams of the above processes are presented, and their advantages and disadvantages are noted. Prospects for further development of these processes are analysed by examples of their practical application.

Keywords: laser technologies, heat treatment, alloying, cladding, coating, hybrid and combined processes, advantages and disadvantages, practical application, prospects for development

Laser-assisted processes are of an increasingly wide interest to deposition of functional coatings [1, 2]. They include laser (cladding and surface modification), as well as hybrid or combined (laser-plasma coating, laser treatment with high-frequency heating, etc.) processes. These processes are implemented by using radiation of technological lasers: gas (CO_2-laser), solid-state (Nd:YAG-laser), diode (Table 1) and fibre ones [3]. Based on the chronology of emergence, the laser-assisted processes can be ranked as follows: heat treatment, alloying, cladding, spraying, and hybrid welding.

Laser heat treatment consists in affecting a workpiece by the focused laser beam, and can be implemented with or without melting of the surface treated. In the latter case, it is necessary to preliminary deposit coatings that absorb the laser radiation [4, 5]. Main advantages of this process include locality of the heat effect (the heating spot is normally 0.1–10.0 mm in size), flexible power supply to the treatment site, and possibility of producing layers with high hardness and wear resistance, modified to a depth from several micrometers to 1–3 mm [6]. As this process is accompanied by refining of grains, it allows hardening of metals without formation of hard phases. Disadvantages of the process include formation of internal stresses along the hardening strips, which may lead to cracking, as well as probability of pore formation in hardening with melting due to evolution of gases caused by burning out of non-metallic inclusions from the base metal [5, 7]. The presence of gases leads to formation of bubbles in the molten pool metal, and because of a short time of existence of the pool the bubbles have no time to escape to the surface.

One of the first ingenious developments utilising to the full extent the optical advantages of laser radiation for the heat treatment processes is special optics, which integrates the energy with the help of a segmented mirror by superimposing many separate elements of the beam [8]. Microprocessor-controlled scanning heads were developed at the end of the 1980s, which were used for laser heat treatment and cladding. Scanning of the laser beam has often been used up to now to uniformly distribute the energy for treatment of complex-configuration workpieces [9], thus providing substantial flexibility of the heat hardening and coating processes.

Laser alloying is intended for forming a comparatively small (approximately 0.2–0.6 mm in diameter and 0.1–3.0 mm deep) molten pool on the surface treated, with metallic and non-metallic (e.g. gaseous) alloying elements added to it [4, 5, 10–12]. As a result of movement of the heat source relative to the surface treated, a layer with modified physical-chemical char-

Table 1. Parameters of different types of high-power lasers used for hardening and coating processes

Laser parameters	CO_2-laser	Pumped Nd:YAG laser		Diode laser
		Lamp-pumped	Diode-pumped	
Wavelength, μm	10.6	1.06	1.06	0.8–0.94
Efficiency, %	5–10	1–3	10–12	30–50
Maximal power, kW	40	4	4	6
Average power density, W / cm^2	$1\cdot10^6$–$1\cdot10^8$	$1\cdot10^5$–$1\cdot10^7$	$1\cdot10^6$–$1\cdot10^9$	$1\cdot10^3$–$1\cdot10^5$
Interval between service maintenances, h	2000	200	10000	10000
Transmission of radiation via optic fibre	No	Yes	Yes	Yes
Quality of radiation, mm·mrad	12	25–45	12	100–1000

acteristics is formed on the latter. Advantages of laser alloying include [4, 5] the possibility of alloying the metal surface to a depth of 2–3 mm to form both chemical compounds and solid solutions of alloying elements in the metal structure, formation of structures with a high dispersion degree and minimal heat-affected zone (HAZ) owing to minimisation of the heat effect on the substrate, and substantial reduction of residual strains, compared with the plasma method. Drawbacks of this process are similar in many respects to those of laser heat treatment. The difference consists in the formation of pores, blowholes and splashes caused by addition of alloying elements (gaseous ones, in the first turn) to the molten pool.

Laser cladding as a method for deposition of coatings originates from laser alloying, which was developed a bit earlier [4, 5, 10–12]. In cladding, a coating of the preset thickness with the preset physical-chemical characteristics is formed on the surface treated due to feeding a cladding consumable (mostly in the form of powder, or more rarely –– in the form of wire) to the zone affected by the laser beam focused into a spot 1–5 mm in diameter. This process may have modifications, including laser cladding on the cladding consumable layers preliminarily deposited on the substrate. These layers are first produced by thermal spraying or by using a covering consisting of a cladding powder and binder, and then they are remelted by using the laser beam [13]. Cladding on the preliminarily deposited layers is usually called laser remelting [14]. The resulting coating adheres to the substrate material through a transition zone of a comparatively small size (5–10 to 50–200 μm) [4]. Strength of adhesion of the coating to the base metal is sufficiently high, and is close to strength of the latter.

One of the important points of the cladding technology is the method of feeding a cladding material onto the substrate. As shown by investigations of laser cladding and welding methods, whereas treatment by the wire cladding process can be realised almost in any spatial position, the advantage of powder consumables consists in a more efficient absorption of laser radiation [15]. Flat cladding can be performed by preliminarily distributing the powder over the surface treated [16]. Application of powder consumables in other spatial positions normally requires that the coatings be deposited by flame [17] or plasma spraying [18], or by furnace drying of the paste-like covering [19]. If a powder cannot be preliminarily distributed over the surface of a workpiece, it should be fed by using special feeders during the cladding process. At present, a wide acceptance has been received by laser cladding using powder additives fed directly to zone affected by the laser beam from special powder feeders of different designs [20].

Advantages of laser cladding include the possibility of deposition of the clad layers with preset properties from 0.1 to 3.0 mm thick [4, 5]; considerable mitigation of the effect of redistribution of components from the substrate material to deposited layer, thus providing a better accuracy of prediction of the results and properties of the deposited layers as close as possible to those of the base material [4, 19]; formation of equiaxed fine-crystalline (highly refined) structures of the deposited metal and a small size (up to 0.1–0.5 mm) of HAZ [21]; and minimisation of allowance for final machining, the size of which is about 0.3–0.5 mm on each side, due to a low (200–300 μm) roughness of the surface treated [22, 23].

Drawbacks of laser cladding include the presence of transverse cold microcracks in the deposited and microlalloyed layers, which are formed as a result of relaxation of high tensile stresses [14]; possibility of formation of both internal and external pores caused by the presence of non-metallic inclusions, residual moisture contained in the cladding powder and contamination of the surface treated; and comparatively high cost of the process resulting from a high cost of laser equipment [4, 5]. The issues of monitoring, decreasing and complete elimination of cracking in laser cladding were investigated in different times by many authors (e.g. [4, 5, 14]). Comparatively recently, the Ukrainian scientists have suggested a mathematical model for this phenomenon, which relates distance between the cracks to mechanical properties of the coatings and their thickness [24]. As follows from the above-said, the promising methods for elimination of the process drawbacks are those that combine reduction of residual thermal stresses in the deposited layers and careful preparation of the powder additives and surfaces being treated. Such methods include, in particular, modification of the thermal cycle of the cladding process through using an additional heat source (e.g. the laser beam combined with the plasma jet).

Laser cladding is used to produce wear- and corrosion-resistant microcrystalline, amorphised and amorphous coatings from a very wide range of materials [21]. However, in the first half of the 1980s the laser cladding technology was applied primarily for repair of worn-out parts operating under conditions of sliding friction, impact loads, abrasive wear, etc. [4, 5, 22, 23]. Reconditioning laser cladding has not lost its topicality up to now even in industrialised countries [25]. Moreover, the technology was developed for underwater laser cladding [26].

Intensive research was carried out in the 1980s on the process of laser thermal spraying [27, 28]. But as the coatings produced by this method were close in their properties to those produced by plasma welding methods, further on this process became less popular than laser cladding. Spraying consumables for this process are powders and wires fed at a speed of 0.5–11.0 m / min (Figure 1). Spraying can be carried out at a speed of 0.5–5.0 m / min and distance between the head and workpiece equal to 50–150 mm by using the 1–5 kW CO_2-laser [27]. The process gas fed at a pressure of 0.1–0.5 MPa can be either inert (e.g. argon) or reactive (nitrogen, oxygen). There is a modification of powder spraying by laser, which includes heating of a spraying powder with the laser beam [28].

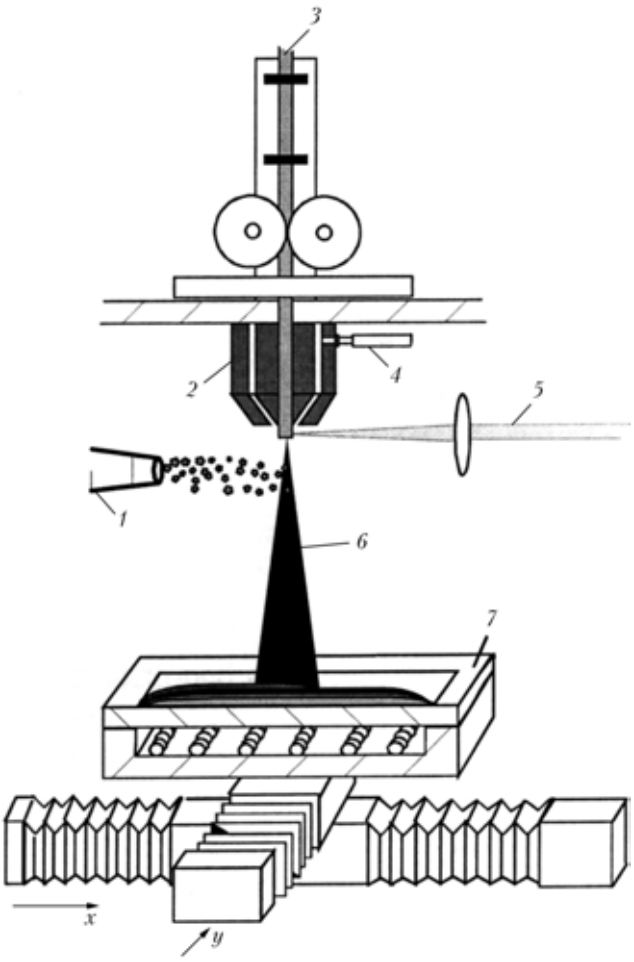

Figure 1. Flow diagram of the laser spraying process involving wire spraying and powders additionally fed to produce composite coatings: *1* — powder feed; *2* — nozzle; *3* — spraying wire; *4* — gas; *5* — laser beam; *6* — spraying jet; *7* — substrate

Differences between the processes of flame spraying, laser cladding and laser powder spraying are demonstrated in Figure 2. With laser cladding the heating spot is just a bit smaller than with laser spraying. However, in the latter case there is no direct impact by the beam on the substrate, which increases locality of the heat effect. Strength of adhesion of the sprayed layers to the substrate is inversely proportional to thickness of the layers. Study [29] dedicated to mathematical modelling of laser powder spraying presents the calculations made for the two most promising modifications of the process, i.e. with coaxial feed of the radiation and powder, and with heating of the powder by the radiation (Figure 2, *c*).

The process flow diagram shown in Figure 1, using wire feeding without a powder, was employed for laser spraying of titanium and titanium nitride on a steel substrate by spraying titanium wire in the Ar + N_2 gas mixture to produce heat-resistant coatings [30]. Because of a lower cost of wire compared with powders, the use of wire for laser spraying allows the cost of this process to be reduced. However, it should be noted that coatings deposited by this method are close in their properties to those produced by arc metallising [31]. Advantages of laser spraying are similar to those of the thermal (e.g. microplasma) spraying processes [32]. The major drawbacks of this process are the necessity of subjecting the surface treated to preliminary jet-abrasive blasting, and a much lower strength of adhesion of the deposited layers to the substrate, compared with laser cladding.

At present the laser spraying method is applied to produce thin coatings with the amorphous or crystalline microstructure, having roughness that matches roughness of the surface treated [33]. Such coatings are characterised by properties of both metals and semiconductors. Another promising area of development of this method is deposition of ceramic coatings, i.e. laser spraying of aluminium oxide [34]. In this case the coatings can be applied to a sub-layer, e.g. of nickel alloys.

Another aspect of application of laser spraying is precision synthesis of 3D parts. The authors of study [35] propose to use robot to produce almost any 3D parts from metal, ceramic or polymer powders. The synthesis processes were developed on the basis of selective laser sintering [36]. One of the most promising areas today is the DMD (direct metal deposition) technology, which is employed most often for manu-

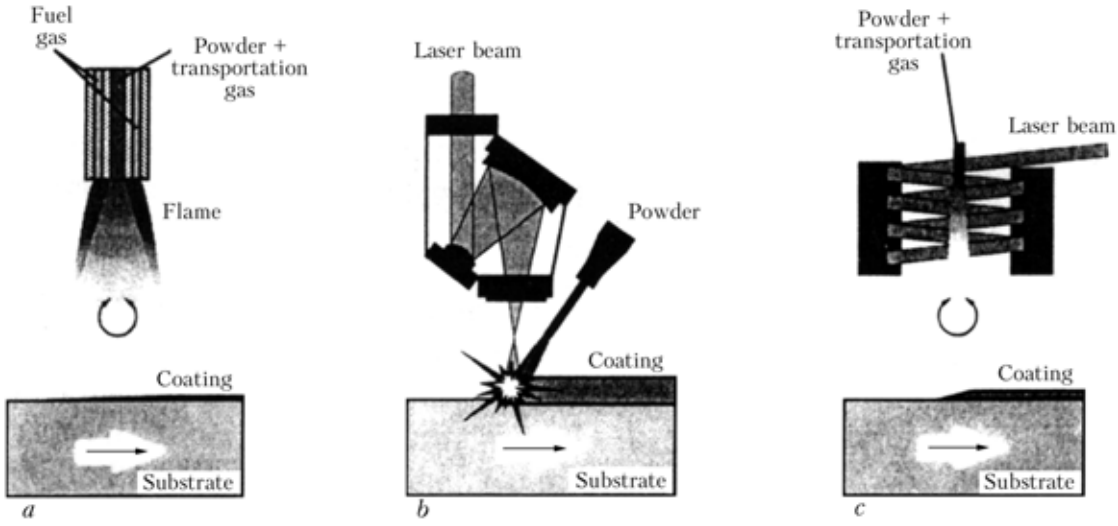

Figure 2. Flow diagrams of the processes of thermal spraying (*a*), laser cladding (*b*) and laser powder spraying (*c*) [26]

facture of dies and moulds (Figure 3). In contrast to the process described in [35], the DMD technology can be regarded as 3D laser cladding, rather than spraying. During the DMD process the laser beam is focused on a metal billet, i.e. 3D mould (a piece that approximately copies the shape of a workpiece), or on a damaged metal part, where it forms the molten metal zone. A thin jet of the metal powder is injected with the help of a transportation gas to the molten zone. The all-metal part is formed layer by layer as a result of computer-controlled movement of the laser beam and powder jet in accordance with the CAD (computer aided design) model.

Another method of laser coating is vacuum laser deposition, which is also called the laser-plasma spraying. When using the modulated laser beam, duration of its pulses may be 60–350 s at a power density of up to 2–5 GW / cm^2. This method is employed to spray thin (less than a micrometer) films. Examples of surface deposition of films can be thin films of high-temperature superconductors, films of such materials as GaAs, InGaAs, PbTe, Bi, ZrO_2, $SrTiO_3$, ZnO, as well as diamond-like films [37]. Thin surface films are produced by using laser radiation in the CVD (chemical vapour deposition) and PVD (physical vapour deposition) processes [38]. As a rule, here the laser beam plays an auxiliary role to improve the existing processes, which can be seen from their names: LACVD (laser assisted CVD) and LEPVD (laser enhanced PVD). Advantages of these processes include the possibility of achieving high physical-mechanical properties of a coating, formation of surfaces that need no subsequent finishing and have roughness identical to that of the substrate; and drawbacks include the presence of special chambers and vacuum equipment, complexity of preparation of a workpiece for coating deposition, and undesirable deposition of a consumable on the surface of the equipment inside the vacuum chambers.

Development efforts are active now on such combined processes as cladding, coating and heat treatment performed by laser with concurrent high-frequency heating [39]. The process of laser induction cladding can be implemented by the similar flow diagram (Figure 4) at the presence of a feeder that feeds a cladding powder.

One of the examples of application of laser induction heat treatment is surface remelting of cast iron cams to produce a wear-resistant ledeburite layer. The high-frequency process component allows eliminating internal residual stresses and microcracks in the modified layer. It is this factor (along with the possibility of considerably increasing the speed of treatment or decreasing the laser power) that is the main advantage of the laser induction processes. Their drawbacks include volumetric heating of a workpiece to high (500–1000 °C) temperatures, which may lead to thermal deformations. Therefore, it is reasonable to apply the combined laser-induction treatment to axisymmetric pieces (e.g. bodies of revolution). Another drawback

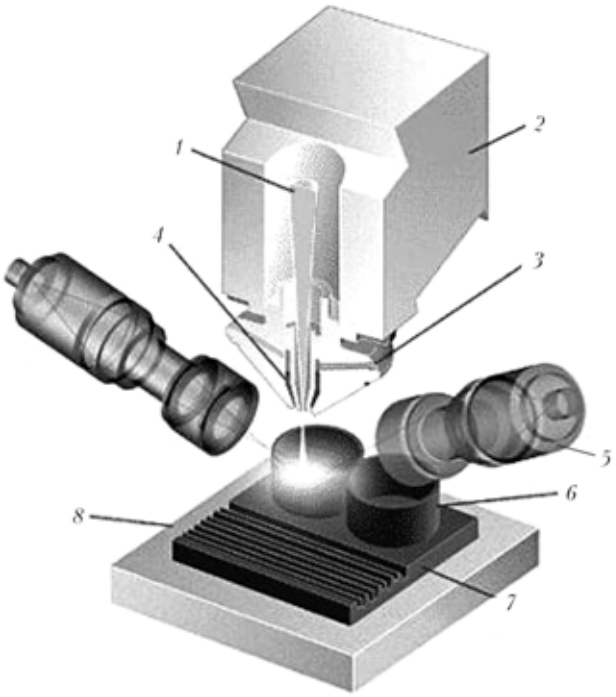

Figure 3. Flow diagram of the process of 3D synthesis of parts by the DMD technology: *1* — CO_2-laser radiation; *2* — focusing optics; *3* — powder feeding; *4* — shielding gas; *5* — sensors of optical feedback system; *6* — piece being formed; *7* — billet or mould; *8* — platform

is a high energy intensity of the combined process. The constant electric field can also be used in such processes, in addition to the high-frequency electromagnetic field.

Modifications of the combined treatment involving laser radiation are laser-light technologies [40]. The light-beam technologies were actively developed in the 1970–1980s [41]. The light-beam treatment methods are applied to advantage for welding and brazing (e.g. car radiators). But this process is of the highest

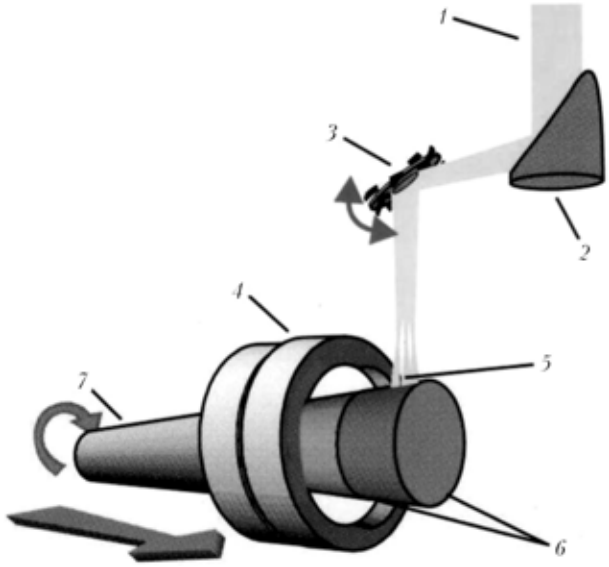

Figure 4. Flow diagram of laser induction heat treatment and cladding with concurrent high-frequency heating [39]: *1* — laser radiation; *2*, *3* — focusing and scanning optics, respectively; *4* — inductor; *5* — shaped laser beam; *6* — workpiece regions heated by means of inductor; *7* — workpiece

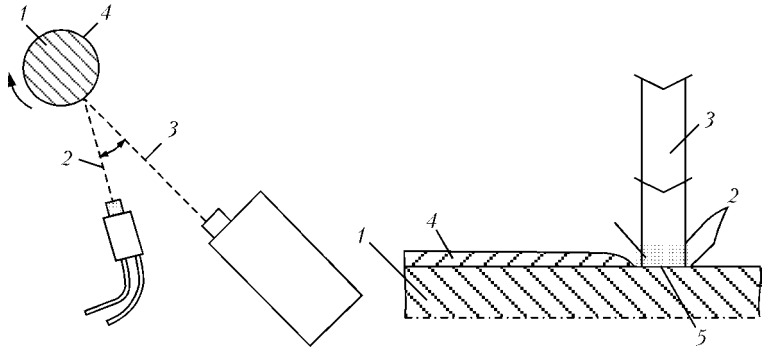

Figure 5. Flow diagram of combined laser-plasma spraying of coatings [46]: *1* — sample; *2* — powder transporting plasma jet; *3* — laser radiation; *4* — deposited layer; *5* — coating formation zone

interest to heat treatment, including the combined laser-light one [40]. In the latter case the light-beam heating plays the same role as the induction or electric one, although it has such a drawback as increased power intensity.

In the last decade the purely laser technologies have been progressively replaced by the hybrid and combined ones. They include the laser-plasma processes using the combined action of the arc plasma and laser heat source. Investigations of the processes of interaction of the focused CO_2-laser beam with the electric arc plasma column, which were conducted by the E.O. Paton Electric Welding Institute, show that a special type of the gas discharge, i.e. the combined laser-arc one, can be formed in this system [42]. Its properties differ from properties of both electric arc and optical discharge maintained by laser radiation. Ability of the combined discharge to generate the high-temperature plasma with a high degree of non-equilibrium (non-isothermicity) even at the atmospheric pressure of an ambient gas makes it attractive for application with plasma-chemical technologies, including the CVD ones. Theoretical and experimental studies conducted by the E.O. Paton Electric Welding Institute show that the above properties of the combined discharge can be used as a basis for development of a new class of plasma devices, i.e. integrated laser-arc plasma torches [43, 44]. A range of integrated laser-arc direct- and indirect-action plasma torches, which are unique for the world practice, is available for such new hybrid processes as laser-microplasma welding, cladding and spraying, as well as hybrid laser-plasma deposition of diamond and diamond-like coatings developed by the E.O. Paton Electric Welding Institute [44].

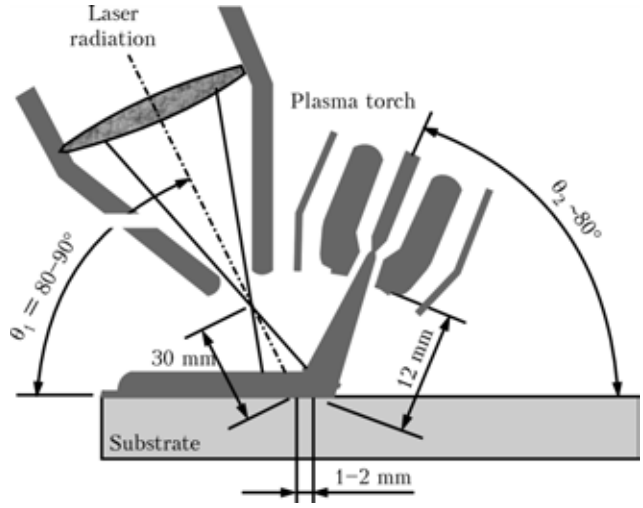

Figure 6. Flow diagram of the optimised proportion of geometric parameters of the process of laser-plasma powder cladding using Nd:YAG laser radiation (workpiece — anode) [54]

The trend in development of the laser-plasma processes is towards modification of surfaces and deposition of coatings 0.1–3.0 mm thick [45, 46]. Laser-plasma hardening and thermal strengthening are a striking example of surface modification [45]. This process is similar in many respects to laser heat hardening [4–6]. The main difference lies in the possibility of replacing a certain portion of the laser energy by the arc plasma energy. Of high interest are the processes of laser-plasma spraying (Figure 5). They combine the effect of laser heating of the surface and plasma coating deposition, where focusing spot *3* of the laser beam is combined with coating formation zone *5* (Figure 5) [46]. This technology is called the laser assisted atmospheric plasma spraying [47]. This process provides a dense layer characterised by increased adhesion strength. Companies LERMPS-IPSe and IREPA-Laser developed and patented the PROTAL technology, which provides the effect of surface preparation by ablation of the substrate surface layer due to incomplete overlapping of the plasma spraying zone by the laser heating zone. As a result, there is no need to use jet-abrasive blasting [47, 48].

Following the Japanese and French scientists [48], investigations of the laser-plasma spraying process were also carried out in Germany (Fraunhofer Institute), Russia and Ukraine. In particular, the plasma-laser fixture and technologies for production of coatings by using dynamic focusers were developed in Russia [49]. The Ukrainian scientists [50] suggested a mathematical model, describing motion and heating of powder particles in laser, plasma and hybrid spraying.

Experiments were conducted on application of the combined laser-plasma processes for depositing cutting tools with the coatings characterised by increased heat and wear resistance, as well as decreased coefficients of sliding friction under contact service loads [45].

Table 2. Comparison of characteristics of laser and thermal spraying processes

Coating process characteristic	Thermal spraying	Laser coating
Heat source	Gas flame, electric arc or plasma	High-intensity laser radiation
Coating to substrate bond	Mechanical bond of low or moderate strength*	High-strength metallurgical bond
Coating structure	Lamellar; from porous to almost dense*	Dense; crack- and pore-free layers
Thermal load on working zone	Low temperature of heating*	Insignificant heating
Dilution of substrate metal	No	Insignificant
Coating thickness	From 0.05 to several millimetres	0.5–3.0 mm
Coating material	Wide range of metals, alloys, hard metals, ceramics and polymers*	Metals and alloys; alloys with hard particles; hard metals; ceramics
Productivity	From low to high*	From low to moderate / (high)*
Cost	From low to high*	From moderate to high

*Depending upon the process type.

In Ukraine, the priority in the field of combined laser-plasma deposition of coatings belongs to the E.O. Paton Electric Welding Institute, which has been active in this area since the beginning of 2000 [44]. Initially, the investigations were conducted by using continuous CO_2-lasers, in contrast to the foreign developments involving pulsed Nd-YAG laser [46] or continuous Nd:YAG and diode lasers [51]. At present, the E.O. Paton Electric Welding Institute is mastering the laser-plasma coating techniques by using the above types of the lasers. The hybrid coating method, where the laser beam is transmitted along the plasma axis, is more advanced in terms of a combined use of the laser and plasma energy [42, 43, 52]. Transportation of the powder material in this case is implemented with preliminary heating by the energy of the laser-plasma discharge [51]. Unlike the hybrid method, the method shown in Figure 5 should be regarded as a combined one. In this case, only the plasma energy is used to heat the spraying powder.

The laser-plasma cladding technology is being upgraded now, in addition to the laser-plasma spraying one. This process uses the direct-action plasma torches and mostly powder consumables [53]. Its main advantage is additional constriction of the plasma arc by the focused laser beam (Figure 6). The authors of study [54] are of the opinion that the pulsed radiation of Nd:YAG-lasers is most promising for this purpose, as it can be flexibly fed via an optic fibre in the optimised spatial position. Compared with laser cladding, the laser-plasma cladding process makes it possible to substantially reduce residual stresses in the deposited layers. However, one of its main drawbacks is still a high thermal effect on a workpiece.

Analysis of advantages and disadvantages of plasma, laser and laser-plasma cladding and spraying processes shows the following. Peculiarities of the majority of the plasma spraying processes are the necessity to employ preliminary surface preparation (most often, jet-abrasive blasting), use of sub-layers in a number of cases, and some discontinuity (microporosity) of the coatings (Table 2).

In the case of plasma cladding, a workpiece may experience a high heating, which leads to residual thermal deformations. The laser and laser-plasma processes make it possible to minimise heating of a workpiece, increase the strength of adhesion of the deposited layers to the substrate, use no sub-layers, and simplify the surface preparation operation. At the same time, the laser cladding processes have some drawbacks, such as the stressed state of the deposited layers and presence of pores and microcracks in them. The hybrid (combined) laser-plasma processes are partially or fully free from the above drawbacks, which is provided by interaction of their components or their combined effect on workpieces. For example, constriction and stabilisation of the plasma arc by laser radiation allows increasing the process speed and decreasing the total heat input; preliminary heating of the powder with the combined discharge, along with modification of the thermal cycle of the laser treatment process due to addition of the plasma component, allows reducing residual stresses, eliminating pore and crack formation; and cleaning of the workpiece surface by laser ablation and its melting make the preliminary surface preparation operation simpler, etc.

Therefore, analysis of the processes of laser and hybrid (combined) hardening and coating deposition shows that owing to their application it has become possible to produce corrosion- and wear-resistant coatings with improved physical-mechanical properties, provide synthesis of 3D objects, and deposit thin films (e.g. diamond and diamond-like) characterised by special properties. Prospects for further development of the laser-plasma (laser-arc) processes of surface modification and coating deposition relate to elimination of drawbacks inherent in each of their components taken separately (laser and arc heat sources), as well as to increase in the efficiency of their interaction.

1. Grigoriants, A.G., Misyurov, A.I. (2005) Possibilities and prospects for application of laser cladding. *Tekhnologiya Mashinostroeniya*, **10**, 52–56.
2. Kovalenko, V.S. (2001) Laser technology at a new stage of development. *The Paton Welding J.*, **12**, 3–8.

3. Vuoristo, P., Tuominen, J., Nurminen, J. (2005) Laser coating and thermal spraying — process basics and coating properties. In: *Proc. of ITSC* (Basel, Switzerland, May 2–4, 2005), 1270–1277.
4. Grigoryants, A.G., Safonov, A.N. (1987) *Laser technique and technology*: Refer. Book. Book 3: Methods of surface laser processing. Ed. by A.G. Grigoriants. Moscow: Vysshaya Shkola.
5. Abilsiitov, G.A., Golubev, V.S., Gontar, V.G. et al. (1991) *Technological lasers*: Refer. Book. Vol. 1: Calculation, design and service. Ed. by G.A. Abilsiitov. Moscow: Mashinostroenie.
6. Khaskin, V.Yu., Pavlovsky, S.Yu., Garashchuk, V.P. et al. (2000) Properties of hypereutectoid complex-alloyed steels after laser heat treatment. *The Paton Welding J.*, **5**, 51–54.
7. Kanarchuk, V.E., Chigrinets, A.D., Shaposhnikov, B.V. (1995) *Laser technique and technology for hardening and repair of parts and apparatuses.* Kyiv: Ukr. Transport. Univ.
8. Dourte, D., Spawr, N.J., Pierce, R.L. *Optical integration with screw supports.* Pat. 4195913 US. Publ. 04.80.
9. Slusher, R.B. *Single axis beam scanner*. Pat. 4387952 US. Publ. 14.06.83.
10. Abboud, J.H., West, D.R.F. (1991) Processing aspects of laser surface alloying of titanium with aluminium. *Mater. Sci. and Technol.*, 7(**4**), 353–356.
11. Pons, M., Hugon, A., Galerie, A. et al. (1991) Laser surface alloying using metal salt precursors. *Surface and Coat. Technol.*, 45(**1–3**), 443–448.
12. Katayama, S., Matsunawa, A., Arata, Y. (1986) Laser nitriding and hardening of titanium and other materials. In: *Proc. of Int. Conf. on Electron and Laser Beam Welding* (Tokyo, July 14–15, 1986). Oxford, 323–324.
13. Pokhmurska, H.V., Dovhunyk, V.M., Student, M.M. (2003) Wear resistance of laser-modified arc-sprayed coatings made of FMI-2 powder wires. *Mater. Sci.*, 39(**4**), 533–538.
14. Pokhmurska, G.V. (2003) Crack formation in thermal coatings depending on conditions of their laser remelting. *Fiz.-Khim. Mekhanika Materialiv*, **1**, 59–62.
15. (2007) Laserstrahlschweissen mit pulverfoermigem Schweisszusatz. *Praktiker*, **3**, 68–69.
16. Steen, W.M., Courtney, C.G.H. (1980) Hardfacing of nimonic 75 using 2 kW continuous wave CO_2-laser. *Metals Technol.*, June, 89–93.
17. Irons, G.C. (1978) Laser fusing of flame spray coatings. *Welding J.*, **12**, 156–161.
18. Ayers, J.D., Schaefer, R.J. (1979) Consolidation of plasma-sprayed coatings by laser remelting. *Laser Applications in Materials Processing*, **198**, 142–148.
19. Matthews, S.J. (1983) Laser fusing of hardfacing alloy powders. In: *Proc. of ASM Conf. on Lasers in Materials* (Florida, USA, Nov. 1983), 138–148.
20. Zeng Xaoyan, Zhu Beidi, Tao Zengyi et al. (1993) Automatic powder feeders and technology of laser cladding. *Chin. J. Lasers*, 20(**3**), 210–214.
21. Zavestovskaya, I.N., Igoshin, V.I., Kanavin, A.P. et al. (1993) Theoretical study of the processes of laser amorphisation and production of microcrystalline structures. *Trudy FIAN*, **217**, 3–12.
22. Arkhipov, V.E., Birger, E.M., Smolonskaya, T.A. et al. (1985) Application of laser technology in repair production. *Svarochn. Proizvodstvo*, **1**, 7–8.
23. Grigoriants, A.G., Safonov, A.N., Shibaev, V.V. et al. (1984) Laser cladding of valve faces of internal combustion engine. *Ibid.*, **5**, 19–20.
24. Chekurin, V.F., Pokhmurska, G.V. (2004) Mathematical model of cracking of laser-modified metal-powder coatings. *Fiz.-Khim. Mekhanika Materialiv*, **5**, 18–22.
25. Hoffman, J. (2001) Reconditioning of exchangeable parts using laser technologies. *The Paton Welding J.*, **12**, 33–34.
26. White, R.A., Fusaro, R., Jones, M.G. et al. (1997) Underwater cladding with laser beam and plasma arc welding. *Welding J.*, **1**, 57–61.
27. Yoneda, M., Utsumi, A., Nakagawa, K. et al. (1988) Fundamental study on thermal spraying by laser. In: *Proc. of ATTAC* (Osaka, May, 1988), 137--142.
28. Wolf, S., Volz, R. (1996) Das Laserstrahlbeschichten integrierbarer Oberflaechenschutz fuer ein breites Anwendungsspektrum des modernen Maschinenbaus. In: *Proc. of Thermal Spraying Conf.* (Essen, Deutschland, Mar. 1996), 160–163.
29. Bushma, A.I., Vasenin, Yu.L., Krivtsun, I.V. (2005) Modelling of the process of laser spraying of ceramic coatings allowing for scatter of the laser beam by spray particles. *The Paton Welding J.*, **12**, 10–14.
30. Utsumi, A., Matsuda, J., Yoneda, M. et al. (1995) Production of compositionally gradient coatings by laser spraying method. In: *Proc. of ITSC* (Kobe, Japan, May, 1995), 325–330.
31. Yurkevich, S.N., Prishchepov, E.G., Pryadko, A.S. et al. (2006) Application of metallising for repair of aircraft engineering parts from steels 30KhGSR2A and 30KhGSA. *Remont, Vosstanovlenie, Modernizatsiya*, **6**, 32–33.
32. Borisov, Yu.S., Kharlamov, Yu.A., Sidorenko, S.L. et al. (1987) *Thermal spray coatings from powder materials*: Refer. Book. Kiev: Naukova Dumka.
33. Rode, A., Gamaly, E., Luther-Davies, D. *Method of deposition of thin films of amorphous and crystalline microstructures based on ultrafast pulsed laser deposition*. Pat. 6312768 US. Publ. 06.11.2001.
34. Mingxi Li, Yizhu He, Xiaomin Yuan et al. (2006) Microstructure of Al_2O_3 nanocrystalline / cobalt-based alloy composite coatings by laser deposition. *Materials & Design*, **27**, 1114–1119.
35. Uchiyama, F., Tsukamoto, K., Fons, P. (1995) Three-dimensional device fabrication using the laser spray process technique. In: *Proc. of ITSC* (Kobe, Japan, May, 1995), 259–262.
36. Ragulya, A.V. (2001) Selective laser sintering of multilayer oxide ceramics. *Functional Materials*, 8(**1**), 162–166.
37. Varyukhin, V.N., Shalaev, R.V., Prudnikov, A.M. (2002) Properties of diamond films obtained in a glow discharge under laser irradiation. *Ibid.*, 9(**1**), 111–114.
38. Hoking, M., Vasantasri, V., Sidki, P. (2000) *Metallic and ceramic coatings: production, properties and applications*. Moscow: Mir.
39. Brenner, B., Standfuss, J., Fux, V. et al. (2001) *Induktiv unterstuetzte Lasermaterialbaerbeitung*. Dresden: Fraunhofer-Institut fuer Werkstoff- und Strahltechnik.
40. Grigoriants, A.G., Shiganov, I.N., Shilov, S.S. et al. (2005) Laser-light treatment of materials as a new trend in hybrid processes. *Tekhnologiya Mashinostroeniya*, **10**, 37–45.
41. Khorunov, V.F., Shan Tsigo (1995) Welding and soldering using light beam of arc xenon lamps (Review). *Avtomatich. Svarka*, **5**, 48–52.
42. Gvozdetsky, V.S., Krivtsun, I.V., Chizenko, M.I. et al. (1995) Laser-arc discharge: Theory and applications. *Welding and Surfacing Rev.*, **3**.
43. Seyffarth, P., Krivtsun, I.V. (2002) *Laser-arc processes and their applications in welding and material treatment. Welding and allied processes.* Vol. 2. London: Taylor and Francis Books.
44. Borisov, Yu., Bushma, A., Fomakin, A. et al. (2005) Integrated laser-arc plasmatron for laser-plasma spraying and CVD processes. In: *Proc. of 2nd Int. Conf. on Laser Technologies in Welding and Materials Processing* (Katsiveli, Crimea, Ukraine, May 23–27, 2005). Kiev: PWI, 57–59.
45. Melyukov, V.V., Kuzmin, V.A., Chastikov, A.V. et al. (2005) Laser-plasma hardening of surface layers of high-speed steels. In: *Proc. of 7th Int. Pract. Conf.-Exhibition* (St.-Petersburg, 13–16 April, 2005), 156–164.
46. Coddet, C.L.M., Marchione, T. *Process for the preparation and coating of a surface*. Pat. 5688564 US. Publ. 18.11.97.
47. Zreris, R., Nowotny, S., Berger, L.-M. et al. (2003) Characterization of coatings deposited by laser-assisted atmospheric plasma spraying. In: *Proc. of Thermal Spraying Conf.* (Orlando, USA, 2003), 567–572.
48. Coddet, C., Montagon, G., Marchione, T. et al. (1998) Surface preparation and thermal spray in a single step: the PROTAL process. In: *Proc. of 15th ITSC* (Nice, France), Vol. 2, 1321–1325.
49. Chashchin, E.A., Fedin, A.V., Mitrofanov, A.A. et al. (2007) Increase in efficiency of plasma treatment of materials by using an additional power source in the form of laser radiation. In: *High technologies, fundamental and applied investigations:* Proc. of 3rd Int. Sci.-Pract. Conf. on Study, Development and Application of High Tech in Industry (St.-Petersburg, 14–17 March, 2007). St.-Petersburg: PU, 119–120.
50. Borisov, Yu.S., Bushma, A.I., Krivtsun, I.V. (2005) Modelling of movement and heating of powder particles in laser, plasma and hybrid spraying. *Dopovidi NAN Ukrainy*, **1**, 86–94.
51. Beyer, E., Nowotny, S. *Method for applying a coating by means of plasma spraying while simultaneously applying a continuous laser beam*. Pat. 6197386 US. Publ. 06.03.2001.
52. Devoino, O.G., Kardapolova, M.A., Krivtsun, I.V. et al. (2007) Structure and microhardness of coatings of high-chromium cast iron powder in hybrid spraying and plasma spraying with subsequent laser glazing. In: *Proc. of 3rd Int. Conf. on Laser Technologies in Welding and Materials Processing* (Katsiveli, Crimea, Ukraine, 29 May–27 June, 2007). Kiev: PWI, 19–23.
53. Hai-ou Zhang, Ying-ping Qian, Gui-lan Wang (2006) Study of rapid and direct thick coating deposition by hybrid plasma-laser manufacturing. *Surface & Coatings Technol.*, **201**, 1739–1744.
54. Wilden, J., Bergmann, J.P., Dolles, M. (2005) Riporti superficiali laser: aumento di efficienza e flessibilita tramite processi ibridi. *Riv. Ital. Saldatura*, Nov.–Dic., 809–816.

DETERMINATION OF CYCLIC FATIGUE LIFE OF MATERIALS AND WELDED JOINTS AT POLYFREQUENCY LOADING

V.S. KOVALCHUK
E.O. Paton Electric Welding Institute, NASU, Kiev, Ukraine

Procedure and analytical dependences are proposed for calculation of cyclic fatigue life of materials, as well as welded joints at polyfrequency loading by the initial data, corresponding to the single-frequency loading. Conducted experimental verification of the derived dependences on large-scale samples, including welded samples, confirmed their validity in a broad range of variation of polyfrequency loading parameters, the spectrum of which consists of 3–7 components.

Keywords: metal structures, welded joints, polyfrequency loading, cyclic fatigue life, calculation

Elements of bridges, crane beams, products of transportation and power engineering, ships, aircraft and many other metal structures during operation are exposed to simultaneous impact of several alternating loads differing in amplitude and frequency. In the general case these loads, due to the impact of external and inner factors, can vary arbitrarily in time, and be of a random nature. In particular, span structures of bridges are loaded by car and railway transport; offshore deep-water platforms are exposed to sea waves; metal structures of tower type constructions, tubular structures are exposed to the impact of inner and outer pressure, as well as air or gas flows.

With the essential difference in the frequencies of individual loads with a random change of amplitudes and phases, such loading patterns of a complex spectrum can be presented in a simplified form by deterministic polyfequency modes, having a simple cycle form:

$$F(t) = \sum_{i=1}^{n} f_i(t)$$

or polyharmonic modes (Figure 1), in which all the components change by the polyharmonic law:

$$F(t) = \sum_{i=1}^{n} A_i \sin(\omega_i t + \varphi_i),$$

where A_i, ω_i are the amplitudes and angular frequencies of the harmonic components, respectively; φ_i are the initial phases (frequency and initial phase of each component usually are random values in a certain frequency band $\omega_{min} \le \omega \le \omega_{max}$ and phase interval of $0 \le \varphi \le \pi$).

Since individual elements of mechanically coupled systems differ by filtering (selective) properties, the wideband loading spectrum usually excites a relatively narrowband reaction in them. In many constructions only the loads with the lowest frequencies are of prevailing importance, as with increase of component frequency in the above-resonance loading region their levels decrease markedly. This enables a schematic presentation of the actual loading of such items by polyfrequency modes, restricting ourselves to two to seven spectral components in many cases.

At polyfrequency loading the individual components can vary essentially in frequency, so that the fatigue resistance of materials and welded joints can depend not only on the interrelation of component parameters, but also on the nominal frequency values.

The available local and foreign experimental data show that additional superposition of the high-frequency component on the main cycle of variable loading leads to accelerated damage accumulation and intensive lowering of the cyclic fatigue life of materials and welded joints. In particular, at bifrequency loading it is established that the adverse influence of the second component is enhanced with increase of the relative values of its amplitude and frequency [1, 2]. It may be supposed that increase of the load spectrum composition will also be accompanied by lowering of the product life. However, quantitative determination of fatigue resistance of materials and joints at polyfrequency loading is difficult. This is due, first of all to the fact, that the existing approaches to assessment of the material cyclic life at complex alternating loading patterns are usually based on the hypothesis of linear summation of damage. The dependences calculated on its basis are in satisfactory agreement with the experimental data only for some values of relationships of parameters and materials, but in most cases they can lead to considerable errors [3, 4]. Suggestions based on the use of nonlinear dependences of damage summation, energy transformation and energy theory of fatigue fracture do not provide an acceptable accuracy, either [4].

Numerous experimental data obtained on structural steels of different classes and strength levels and their welded joints showed [5] that the coefficient of fatigue life lowering under the conditions of bifrequency loading $\kappa_{1\text{-}2}$ can be found from the following relationship:

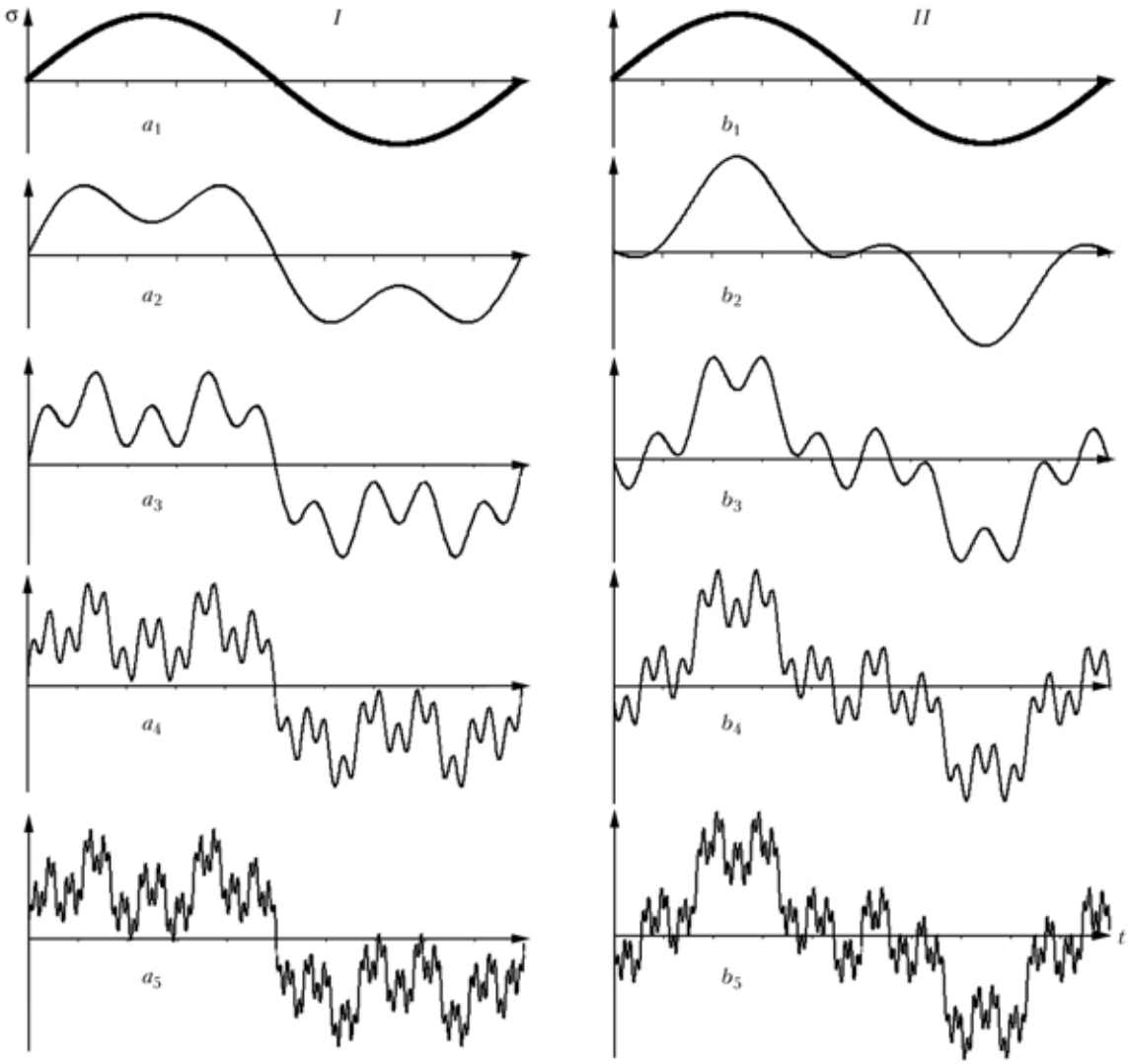

Figure 1. Cycle shape at harmonic a_1, b_1 and polyharmonic loading with 2 (a_2, b_2)–5 (a_5, b_5) components: *I* — initial phases of all the components of $\varphi = 0$; *II* — initial phase of the basic component b_1 is equal to $\varphi = 0$, of all the other phases $\varphi = \pi$

$$\kappa_{1\text{-}2} = N_1 / N_{1\text{-}2} = (f_2 / f_1)^{\vartheta(\sigma_{a2}/\sigma_{a1})}, \quad (1)$$

where N_1, $N_{1\text{-}2}$ are the fatigue lives measured by the number of load cycles up to initiation of fatigue crack of certain size at the same levels of stresses of single-frequency loading and low-frequency component of bifrequency loading, respectively; f_1, f_2 are the frequencies; σ_{a1}, σ_{a2} are the amplitudes of the low- and high-frequency components, respectively; ϑ is the coefficient of proportionality, dependent on the material mechanical properties.

If the material, kind of joint, stress concentration, residual stresses, cycle asymmetry, temperature, fatigue fracture criterion and other conditions of single- and bifrequency loading are identical, coefficient $\kappa_{1\text{-}2}$ is invariant to the above parameters at all the stress levels in the range between the endurance and yield limits of the material. This enables determination of the cyclic life at bifrequency loading $N_{1\text{-}2}$ from the available calculated or experimental values of fatigue life N_1 corresponding to single-frequency loading:

$$N_{1\text{-}2} = N_1 / \kappa_{1\text{-}2}. \quad (2)$$

It may be assumed that a certain dependence of the coefficient of fatigue life lowering exists also at a large number of simultaneously acting alternating loads, i.e. at polyfrequency loading. Then, having the data on the value of this coefficient at the respective parameters of polyfrequency loading, the cyclic life of materials and joints can be determined in a similar fashion. However, finding such coefficients experimentally is complicated by an unlimited number of possible combinations of amplitude, frequencies, and components. In addition, the law of damage accumulation at one or several components of the cyclic stress spectrum has not been established so far, particularly at the stage of fatigue crack initiation.

Establishment of a functional dependence between the parameters of polyfrequency loading and coefficient of variation of cyclic life can be essentially simplified, if the regularities of damage accumulation under the conditions of single- and polyfrequency loading are similar. As regards the bifrequency loading, the conclusion about the similarity of these regularities follows from analysis of the earlier derived results of experimental studies of structural materials and

welded joints. In this case, the invariance of coefficient $\kappa_{1\text{-}2}$ to a number of design, technological and service factors is attributable to similar manifestation of their influence on the fatigue processes both at single- and at bifrequency loading. In the latter case, the cyclic fatigue life decreases only under the impact of an additional high-frequency component, this leading at fixed values of amplitude and frequency relationships to parallel shifting of the initial *S*–*N* curve into the region of lower fatigue life, and of the kinetic diagram of fatigue fracture ---- into the region of higher rates of fatigue crack propagation. Parallel arrangement of *S*–*N* curves or fatigue fracture diagrams points to the fact that the regularities of the processes of damage accumulation on the same levels of single- and bifrequency loading are similar and differ only by the coefficients of proportionality. It follows that at a fixed level of alternating stresses and one fatigue fracture criterion, which a fatigue crack of certain dimensions usually is, the fatigue damage accumulated under the conditions of single- and bifrequency loading, is the same. Evidently, it makes sense to assume a conditional or real fatigue crack of length L as the accumulated damage criterion. In this case, comparison of fatigue testing results can be performed by average values of the levels of accumulated damage from individual alternating load cycles, without allowing for the material damageability kinetics, which depends on many factors for each kind of loading taken separately. Then the average damage rate per one cycle of alternating loading V on σ_a stress level can be found from the following expression:

$$V = L / N, \tag{3}$$

where L is the accumulated damage, equivalent to the real or conditional fatigue crack, expressed in units of length (depth or area); N is the cyclic fatigue life before damage accumulation L, expressed by the number of load cycles.

With such an approach the accumulated damage under the conditions of single-frequency loading can be presented in the following form:

$$L_1 = V_1 N_1, \tag{4}$$

and under bifrequency loading in the form of

$$L_{1\text{-}2} = V_{1\text{-}2} N_{1\text{-}2}. \tag{5}$$

It is obvious that fatigue damage at bifrequency loading is caused by the simultaneous action of N_1 cycles of the basic, usually low-frequency loading, and N_2 cycles of superposed load smaller in magnitude, but of a higher frequency. In this case, the total damage value is equal to

$$L_{1\text{-}2} = L_1 + L_2. \tag{6}$$

Considering that in order to determine the coefficient of fatigue life lowering at bifrequency loading, the compared cycle numbers N_1 and $N_{1\text{-}2}$ should be selected at the same values of fatigue crack lengths $L_1 = L_{1\text{-}2}$, equality of their values $V_1 N_1 = V_{1\text{-}2} N_{1\text{-}2}$ taking into account expression (1) yields the following dependence:

$$V_{1\text{-}2} / V_1 = \kappa_{1\text{-}2}. \tag{7}$$

From expression (7) it follows that the average rate of fatigue damage accumulation at bifrequency loading is $\kappa_{1\text{-}2}$ times higher than at single-frequency loading. To evaluate the degree of the influence of each component of bifrequency loading on the process of fatigue damage accumulation, it is necessary to compare the damage accumulated under the conditions of single- and bifrequency loading at the same number of cycles of single-frequency loading and low-frequency component of bifrequency loading, i.e. $N_1 = N_{1\text{-}2}$. Then the damage from the low-frequency component L_1 can be found from expression (4), and that from high-frequency component L_2 ---- from relationship

$$L_2 = L_{1\text{-}2} - L_1 = V_{1\text{-}2} N_{1\text{-}2} - V_1 N_1 = N_1 (V_{1\text{-}2} - V_1).$$

After replacement in this expression of $V_{1\text{-}2} = V_1 \kappa_{1\text{-}2}$ by its value from expression (7), damage L_2 can be expressed as $L_2 = N_1 V_1 (\kappa_{1\text{-}2} - 1)$, and taking (4) into account ---- in the form of

$$L_2 = L_1 (\kappa_{1\text{-}2} - 1). \tag{8}$$

This expression shows that the process of fatigue damage accumulation L_2 from the additional high-frequency component proceeds $(\kappa_{1\text{-}2} - 1)$ times more intensively than that from the basic low-frequency component of bifrequency loading. On this basis total damage caused by simultaneous action of the low- and high-frequency components of bifrequency loading, can be presented as

$$L_{1\text{-}2} = L_1 + L_1 (\kappa_{1\text{-}2} - 1) = L_1 \kappa_{1\text{-}2}, \tag{9}$$

and the average rate of their accumulation in the form of

$$V_{1\text{-}2} = L_1 \kappa_{1\text{-}2} / N_{1\text{-}2}. \tag{10}$$

By analogy with the bifrequency loading, the total fatigue damage accumulated at polyfrequency loading, can be determined as the sum of damage from all the components

$$L_{1\text{–}n} = L_1 + L_2 + \ldots + L_n. \tag{11}$$

After substitution into expression (11) of the respective values and simple transformation, the dependence for determination of fatigue damage at polyfrequency loading $L_{1\text{–}n}$ by the data of single-frequency loading L_1 can be presented in the following form:

$$L_{1\text{–}n} = L_1 \left[1 + \sum_{i=2}^{n} (\kappa_i - 1) \right]. \tag{12}$$

By analogy with dependence (9) the coefficient of lowering of cyclic fatigue life at polyfrequency loading can be found from expression (12) in the following form:

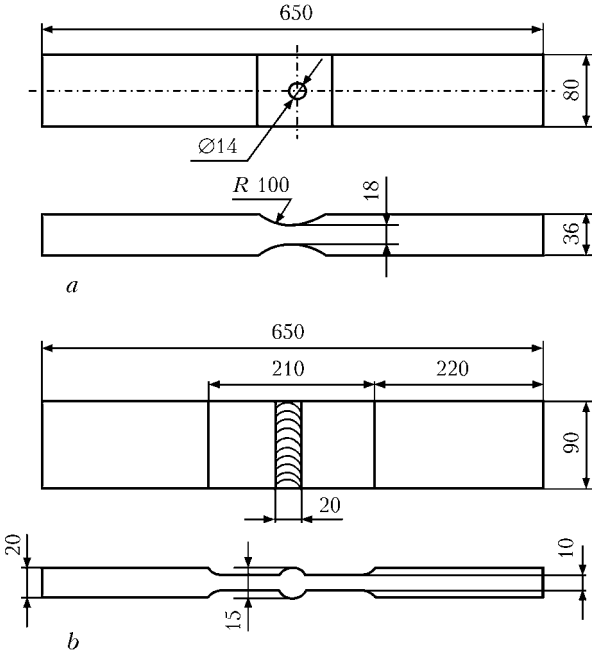

Figure 2. Schematics of samples for fatigue testing at single- and polyfrequency loading from base metal with a central hole (*a*) and with a butt welded joint (*b*)

$$\kappa_{1\text{-}2} = 1 + \sum_{i=2}^{n} (\kappa_i - 1). \qquad (13)$$

This dependence allows determination of cyclic fatigue life at polyfrequency loading N_{1-n} similar to (2) by the following formula:

$$N_{1-n} = N_1 / \left[1 + \sum_{i=2}^{n} (\kappa_i - 1) \right]. \qquad (14)$$

At practical application of expressions (13) and (14) it is important to correctly select the procedure of determination of values κ_i for individual components by expression (1). Two approaches can actually be applied: first is to determine value κ_i relative to a common basic component, which has the largest amplitude of σ_{a1} stresses, i.e. $\kappa_{2,1}$; $\kappa_{3,1}$; $\kappa_{4,1}$, etc., and the second is to determine κ_i value by the ratio of parameters between individual components in the sequence of lowering of σ_{ai} stress amplitudes, i.e. $\kappa_{2,1}$; $\kappa_{3,2}$; $\kappa_{4,3}$, etc.

It is seen from Figure 1 that the greatest change of cycle shape of the basic component (a_1, b_1) is caused by the component second by its level and frequency. The third component has the greatest influence on the cycle shape of the second component, etc. Proceeding from that it may be assumed that at a small number of components there will be no essential differences in finding κ_{1-n} with both variants of κ_i determination. However, at a great number of the components, the second variant will be a preferable, and, therefore, a more general solution.

The final conclusion about the adequacy of the proposed method and selection of the respective variant of determination of κ_i coefficients can be derived based on the results of experimental verification. With this purpose, flat samples (Figure 2) with a central hole, as well as those with a butt welded joint, were made and tested for fatigue at single- and polyfrequency soft axial tension. As noted above, at polyfrequency loading the individual components can differ essentially by frequency, and fatigue resistance of welded joints can depend not only on the interrelation of the component parameters, but also on the nominal values of frequencies. Considering that the degree of the influence of loading frequency on the cyclic life decreases noticeably with increase of strength properties of structural materials [6], in order to eliminate or markedly lower the influence of this factor on testing results, the samples were made of high-strength steel with the yield limit of about 1000 MPa. To derive initial data under the conditions of zero-to-tension single-frequency loading, fatigue testing of base metal samples was performed at the frequencies of 3, 30 and 300 cycles per minute, included into the frequency range, in which the greatest change of fatigue resistance is usually observed, and which covers the frequencies of the main alternating loads of many welded metal structures. At polyfrequency loading the spectrum consisted of several components of different frequency and amplitude. In the real structures, the levels of higher frequency components are lower than those of the basic alternating load, and they usually decrease with increase of the nominal frequency, while the phase shift between them can change arbitrarily in time. Modes of sample testing at polyharmonic loading were assigned in a similar fashion. Ratios of stress amplitudes of three-frequency loading σ_{a1}:σ_{a2}:σ_{a3} were set in the ranges close to 1:0.4:0.2, and ratios of frequencies f_1:f_2:f_3 ---- in the ranges of 1:3:9 and 1:9:81 with zero initial phase of the basic component, and initial phase $\varphi = \pi$ of the other components unfixed during testing. Part of samples with the number of components equal to 4–7 was tested in a similar fashion. Asymmetry and number of cycles at polyharmonic loading were determined by the basic component, having the lowest frequency and highest amplitude. The initial stage of crack propagation was taken as the criterion of fatigue fracture of these samples. During testing the fatigue cracks usually initiated on the inner surfaces of the hole located on the sample horizontal axis, and propagated along the length and depth normal to the applied load. At fatigue cracks coming to the sample side surface and reaching the length of up to 3–4 mm, testing was interrupted. Results of fatigue testing of base metal samples from high-strength steel at single-frequency loading are presented in the graphic form in Figure 3, curve *1*, and at polyharmonic loading ---- in the Table.

Taken as the main kind of welded joint, was a butt weld which is widely accepted in load-carrying structural elements, and has a high fatigue resistance under alternating loading conditions. Dimensions of welded samples (see Figure 2, *b*) were selected from the condition of the possibility of development of high resid-

Results of fatigue testing of samples of base metal and welded joints of high-strength steel at polyharmonic axial tension (r = 0, ϑ = = 1.67)

Samples	Sample loading mode									
	Frequency, Hz							Stresses, MPa		
	f_1	f_2	f_3	f_4	f_5	f_6	f_7	σ_{a1}	σ_{a2}	σ_{a3}
Base metal	1.62	4.86	14.58	–	–	–	–	210	84	43
	0.54	1.62	4.86	–	–	–	–	210	83	84
	0.18	1.62	14.58	–	–	–	–	189	70	25
	0.18	1.62	14.58	–	–	–	–	198	80	41
	0.06	0.54	4.86	–	–	–	–	195	76	40
	0.02	0.18	1.62	14.58	–	–	–	203	77	61
	0.02	0.06	0.18	1.62	14.58	–	–	219	93	65
	0.02	0.06	0.18	0.54	1.62	14.58	–	213	88	62
	0.02	0.06	0.18	0.54	1.62	4.86	14.58	225	67	56
Butt joints	0.54	1.62	4.86	–	–	–	–	154	63	30
	0.54	1.62	4.86	–	–	–	–	141	56	29
	0.54	1.62	4.86	–	–	–	–	132	52	27
	0.54	1.62	4.86	–	–	–	–	95	28	15
	0.18	1.62	14.58	–	–	–	–	84	34	17
	0.18	1.62	14.58	–	–	–	–	123	50	25
	0.18	1.62	14.58	–	–	–	–	140	42	21
	0.18	1.62	14.58	–	–	–	–	158	48	24
	0.02	0.06	0.18	1.62	14.58	–	–	100	41	30
	0.02	0.18	0.54	1.62	4.86	14.58	–	100	38	35
	0.02	0.06	0.18	0.54	1.62	4.86	14.58	120	48	42

Table (cont.)

Samples	Sample loading mode				Cycle number, thou		Coefficient κ		
	Stresses, MPa						Exp.	Calculation	
	σ_{a4}	σ_{a5}	σ_{a6}	σ_{a7}	Polyharmonic	Single-frequency	κ_{exp}	Variant 1 κ_{c1}	Variant 2 κ_{c2}
Base metal	–	–	–	–	25.0	91	3.6	3.20	3.64
	–	–	–	–	14.0	91	6.5	5.41	7.56
	–	–	–	–	20.0	115	5.3	5.48	6.51
	–	–	–	–	14.1	110	7.8	7.98	9.97
	–	–	–	–	6.9	105	15.2	7.69	10.08
	39	–	–	–	2.6	96	36.9	19.22	30.83
	46	23	–	–	3.61	75	20.8	10.00	22.47
	43	32	18	–	2.07	80	38.6	9.63	17.14
	46	31	22	11	2.74	66	24.1	9.21	15.50
Butt joints	–	–	–	–	7.0	32	4.5	3.16	3.51
	–	–	–	–	5.0	44	8.8	3.20	3.66
	–	–	–	–	12.0	60	5.0	3.18	3.65
	–	–	–	–	30.0	80	2.7	2.50	3.39
	–	–	–	–	44.4	250	5.6	7.83	9.68
	–	–	–	–	6.0	70	11.7	7.89	9.71
	–	–	–	–	11.9	44	4.7	5.01	8.27
	–	–	–	–	4.5	28	6.2	5.10	8.31
	15	5	–	–	7.65	60	7.8	6.87	12.60
	29	20	10	–	2.6	60	23.0	24.56	16.10
	40	30	24	12	1.03	30	29.0	22.49	18.60

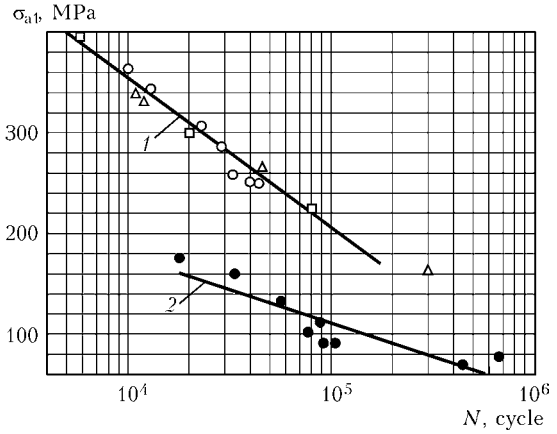

Figure 3. *S–N* curves of samples from high-strength steel with a central hole (*1*) and with a butt welded joint (*2*) at single-frequency axial tension: Δ, ❒, ○ — r = 0, respectively f = 3, 30, 300 min^{-1}; ● — r = 0.3, f = 180 min^{-1}

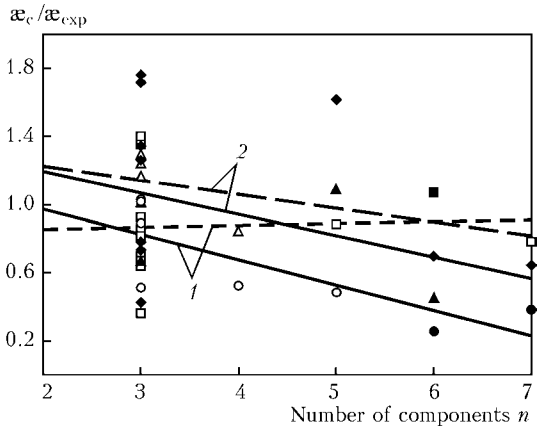

Figure 4. Results of comparison of calculated κ_c and experimental κ_{exp} values of the coefficients of lowering of cyclic fatigue life for samples of base metal (BM) and butt welded joint (BWJ) at polyharmonic loading: *1* — first variant of calculation of BM (●) and BWJ (■), respectively; *2* — second variant of calculation of BM (▲) and BWJ (◆), respectively

ual stresses in them during welding and inducing the required working stresses at fatigue testing in the SCHENCK servohydraulic machine of PC1 type with the force of 1000 kN. Samples were made from sheet high-strength steel of 20 mm thickness. Sample blanks were cut along the rolling direction using Kiev-4 type machine for air-plasma cutting of metal. Plate surfaces were treated by milling with subsequent grinding of the working part to the thickness of 10 mm. Two-sided symmetrical edge preparation was performed at the angle of 45° with 2 mm toe. Sample welding was conducted by DCRP mechanized process. Sv-03GKhN3MD electrode wire of 3 mm diameter and FIMS-20P flux were used as welding consumables. To ensure a high cracking resistance of the metal of the weld and HAZ, sample edges to be joined were preheated to 373 K before welding. Each sample was welded separately in four passes in the horizontal position, and the start and end of the butt weld were located on run-off tabs, welded to the plates before welding. After welding, the run-off tabs were removed by air-plasma cutting, and the side faces were milled.

As the rational use of high-strength steels in welded structures is achieved at asymmetrical axial tension, the characteristic of the cycle of single-frequency and basic component of polyfrequency loading was taken to be equal to r = 0.3. A fatigue crack 3 mm long on the sample surface was taken as the criterion for completion of fatigue testing. Fatigue testing of welded samples at single-frequency loading was conducted under the conditions of soft harmonic axial tension at 3 Hz frequency. Fatigue cracks initiated in the samples along the line of fusion of the weld with the base metal. Results of fatigue testing of welded samples at single-frequency loading are given in Figure 3, curve *2*. Testing modes of welded joints at polyharmonic loading were selected similar to those for base metal samples with three, five, six and seven components (Table). Calculated values of total coefficients of lowering of cyclic fatigue life of base metal and welded joint samples at polyharmonic loading, determined by the first κ_{c1} and second κ_{c2} variants are also shown in the Table. Results of comparison of calculated κ_c coefficients of fatigue life lowering with experimental values κ_{exp} given in Figure 4, show that both the calculation variants yield an acceptable accuracy at polyharmonic loading with 3 to 7 components. However, the second variant of calculation κ_{c2} is preferable, as it provides a certain fatigue life margin at loading with 3 to 5 components. It should be noted that the results of κ_c / κ_{exp} comparison have an increased scatter at first glance. However, in this case it is, probably, difficult to obtain a higher accuracy of experimental κ_{exp} and calculated κ_c values. This is related to a change of the value and nature of the total load cycles, which at low frequency ratios depend not only on the amplitude ratios, but also on the law of the change of phase shift between the components. During loading this regularity is determined by the initial phase shift, as well as the relationship and order of the component frequencies. It is impossible to influence the nature of this dependence under the actual conditions of structure operation. Therefore, the suggested analytical dependencies use formula (1), not allowing for the phase shift between the components and applied at bifrequency loading with frequency ratio of not more than 10, when the phase shift impact can be neglected. However, at aliquant frequency ratios, the phase shift between the components, and, accordingly, the nature and value of the summary load change continuously in time from the minimum to maximum values. In these cases, the effective summary load will, probably, be its value average over the time of impact. At multiple ratios of frequencies and fixed phase shifts between the components (see Figure 1), maximum or minimum κ_{exp} values can be obtained, depending on their initial values. In building metal structures the latter cases are improbable, and under the conditions of fatigue testing in modern equipment with program control, they are quite feasible.

CONCLUSIONS

1. Proposed procedure and analytical dependences allow determination of the coefficients of lowering of

cyclic life of materials and welded joints at polyfrequency loading.

2. Proceeding from the initial data of single-frequency loading and assigned parameters of polyfrequency loading components, it is possible to predict the cyclic fatigue life of metal structure elements under these conditions.

3. Data of experimental studies of cyclic life of steel base metal and butt welded joints derived in this work, confirmed the acceptable accuracy of the procedure and calculated dependencies. At 3 to 7 components of polyharmonic loading the main part of the results of comparison of the calculated and experimental values of the coefficient of cyclic life lowering is in agreement with a not more than 40 % error.

1. Buglov, E.G., Filatov, M.Ya., Kolikov, E.A. (1973) Resistance of materials at bifrequency loading (Review). *Problemy Prochnosti*, **5**, 13–17.
2. Trufyakov, V.I., Kovalchuk, V.S. (1982) Determination of fatigue life at bifrequency loading. Report 1: Review. *Ibid*., **9**, 9–15.
3. Geminov, V.N. (1967) About physical principles of the methods of damage summation under nonstationary loading conditions (Review). In: *Strength of materials at cyclic loads*. Moscow: Nauka.
4. Troshchenko, V.T., Sosnovsky, L.A. (1987) *Fatigue resistance of metals and alloys*: Refer. Book. Pt 1. Kiev: Naukova Dumka.
5. Trufyakov, V.I., Kovalchuk, V.S. (1982) Determination of fatigue life at bifrequency loading. Report 2: Proposed procedure. *Problemy Prochnosti*, **10**, 15–20.
6. Kovalchuk, V.S. (1991) Influence of loading frequency on fatigue resistance of steels and welded joints. *Avtomatich. Svarka*, **1**, 30–34.

IMPROVEMENT OF TRIBOTECHNICAL CHARACTERISTICS OF HARDFACED CAST IRON AUTOMOBILE CRANKSHAFTS

S.Yu. KRIVCHIKOV

E.O. Paton Electric Welding Institute, NASU, Kiev, Ukraine

Influence of heat treatment modes on tribotechnical characteristics of working mating arrangements of hardfaced crankshafts operating under conditions of metal against metal friction with lubrication was assessed. It is shown that tempering temperature influences quantitative ratio between pearlite and carbide-cementite phases in structure of the deposited metal and its wear resistance.

Keywords: arc surfacing, deposited metal, structure and hardness, tribotechnical characteristics, heat treatment

A crankshaft is the most loaded part of the internal combustion engine (ICE). Main loads, which determine its service life, are high contact pressure in rubbing mating arrangements and big number of alternating load cycles. This causes irregular wear and misalignment of working surfaces, violation of oil film, and creation of conditions for dry and marginal friction. As a result «seizure» and melt-out of inserts, mated with hardfaced crankshaft journals, may occur.

In repair production technology of wide-layer surfacing using the PP-AN160 self-shielded flux-cored wire is widely used for renovation of worn cast iron ICE crankshafts [1]. The deposited metal represents a wear-resistant high-carbon alloy, the crankshaft base metal is cast iron of the VCh 50-2 grade (ChShG) hardened for pearlite structure. Chemical compositions of the base and the deposited metal are given in Table 1.

Experience of operation and repair of the hardfaced crankshafts shows that wear resistance of the hardfaced journals exceeds that of the base metal, but wear of the mated with the hardfaced journal insert occurs more intensively than of the deposited metal.

Purpose of this work is experimental investigation of influence of the deposited metal heat treatment on tribotechnical characteristics of working mated arrangements of crankshafts.

Testing of friction–sliding pairs with a lubrication was performed on the SMT-1 friction machine according to the «roller–block» scheme in agreement with GOST 23224–86. Segments from standard automobile AO 20-1 inserts were used as the blocks. For manufacturing of the rollers (Figure 1) billets from ChShG were used, cylindrical surface of which was hardfaced using the PP-AN160 flux-cored wire, then they were

Table 1. Chemical composition of deposited and base metal, wt.%

Alloy investigated	C	Cr	Si	Mn	Ti	Al	B	Mg
Deposited metal	2.4	0.3	1.8	0.8	0.3	0.5	0.08	–
Base metal (ChShG)	2.8	0.2	2.1	1.3	–	–	–	0.03

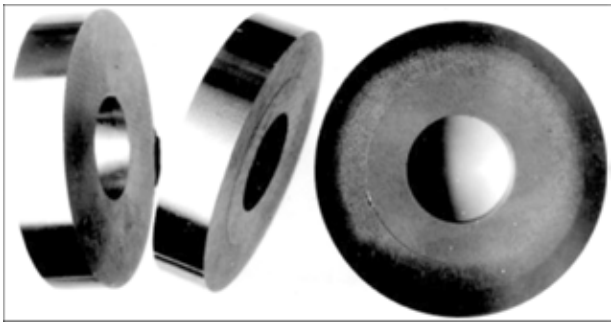

Figure 1. Roller for determining tribotechnical characteristics of friction–sliding pairs: external diameter of 50 mm, thickness of 12 mm

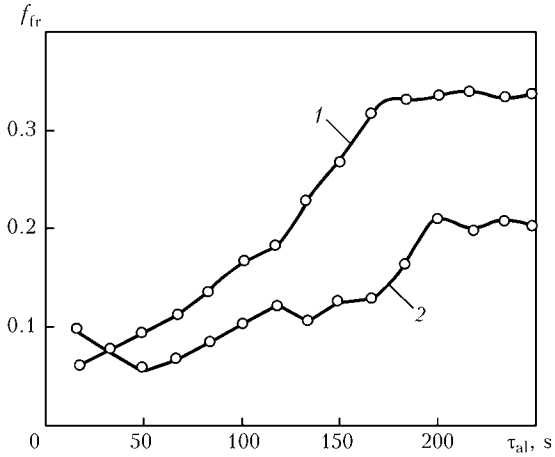

Figure 2. Change of friction factor upon time of aligning of the base metal–insert (*1*) and deposited metal–insert (*2*) mating arrangement after heat treatment at T_{temp} = 520–550 °C (*2*) at v_{sl} = = 0.8 m / s

subjected to heat treatment and grinding up to nominal dimensions. Heat treatment was performed under following conditions: heating in the furnace up to the assigned temperature, soaking at this temperature for 2 h, and cooling in quite air.

Testing of friction pairs was performed in two stages: under conditions of alignment of mating parts and at the working load. Optimum working load P_{op} was chosen on basis of preliminary experiments which showed that its excess could cause «seizure» of the mating arrangements. Total intensity of wear of the mating arrangements as a whole I_Σ was determined as total of intensity of wear of the insert I_i and the roller I_r (methodology for determining these values is given in GOST 23.224–86). In addition, in the process of the tests recording of the friction factor change f_{fr} (Figure 2) and temperature of the oil friction heating T_{fr} was performed. The results obtained (Table 2) prove that heat treatment exerts significant influence on tribotechnical characteristics of both deposited metal and the insert and the mating arrangement as a hole. One may see from comparison of intensities of wear of mating arrangements 1 and 2 that wear resistance of the deposited metal exceeds that of the base metal, but intensity of the insert wear I_i in mating arrangement 2 is 2.2 times higher than in mating arrangement 1. According to other indices of wear resistance and serviceability the ChShG–insert friction pair also exceeds the deposited metal–insert mating arrangement.

After heat treatment at T_{temp} = 400–420 °C tribotechnical properties of mating arrangement 2 insignificantly improve: values I_i, I_Σ, f_{fr} and T_{fr} reduce, and P_{op} increases. By means of T_{temp} increase up to 520–550 °C listed parameters undergo significant changes and achieve values at which mating arrangement 2 in all tribotechnical parameters exceeds mating arrangement 1. Further increase of T_{temp} causes significant worsening of the deposited metal wear resistance and serviceability of the mating arrangement as a whole.

For determining reasons of change of tribotechnical characteristics of mating arrangements at heat treatment of the deposited metal the metallographic investigations were carried out. It should be noted that detailed analysis of structural-phase state of the multicomponent alloy, solidification of which occurred under non-equilibrium conditions, is a rather labor-consuming task. However, it was established with sufficient degree of accuracy that structure of the deposited metal consisted of two main phases: products of austenite decomposition (pearlite + residual austenite) and carbide-cementite phase. The latter in plane of the section had an appearance of a branched reinforcing mesh with areas of different thickness. In Figure 3 this phase has white color, while pearlite-austenite phase has dark color which made it possible to evaluate their quantitative ratios.

Table 2. Tribotechnical characteristics of friction–sliding pairs

Mating arrangement	Type of mating	Indices of serviceability		Intensity of wear, mm / m·10^{-4}			$f_{fr}\cdot10^{-2}$
		P_{op}, MPa	$\dot{O}_{fr}$, $^i\tilde{N}$	I_r	I_i	I_Σ	
1	Base metal ChShG–insert	16.0	60	0.29	0.12	0.41	35
2	Deposited metal–insert						
	without heat treatment	11.0	72	0.24	0.26	0.50	45
	after heat treatment at T, °C:						
	400–420	11.6	68	0.24	0.24	0.48	42
	520–550	14.0	50	0.22	0.12	0.34	20
	650–700	9.5	80	0.49	0.10	0.59	68

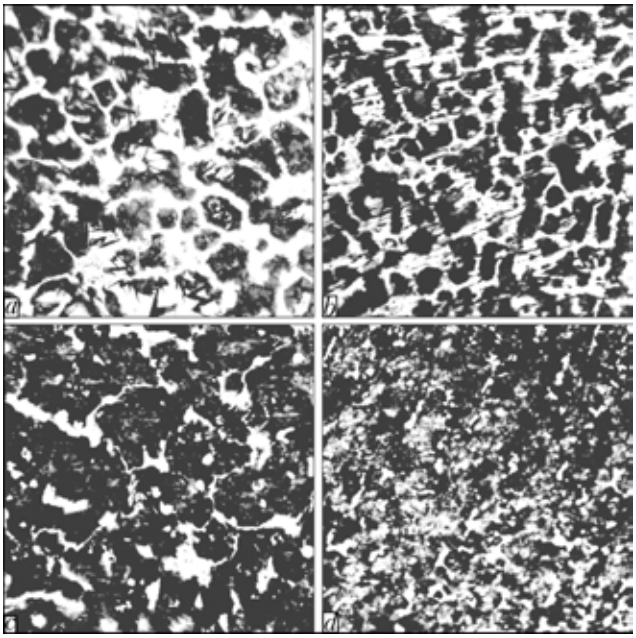

Figure 3. Influence of heat treatment on structure of deposited metal: *a* — without heat treatment; *b*–*d* — at T_{temp} = 400–420, 520–550 and 700–750 °C, respectively (×320)

It was established that by means of increase of the tempering temperature carbide-cementite mesh first gets thinner, then gets torn, and, at last, disintegrates into separate inclusions of cementite. In initial state (without heat treatment) the deposited metal contains 40–46 % of «white» (carbide-cementite) phase of hardness *HV*0.5-8000–8200 MPa. Microhardness *HV*0.5 of the solid solution grains («dark phase») is 5800–6200 MPa. As a result of heat treatment at temperatures 520–550, 650–700 and 800 °C the share of carbide-cementite phase constituted 28–33, 21–25 and 8–12 % respectively, and its hardness remained unchanged.

By means of increase of T_{temp} microhardness of pearlite monotonously diminished from *HV*0.5-5200–5400 (at T_{temp} = 400 °C) to *HV*0.5-4200–4400 (at T_{temp} = 800 °C) which is connected with a partial decomposition of secondary cementite into iron and graphite at heating [2]. Influence of tempering temperature on hardness of the deposited metal is presented in Figure 4. Reduction of hardness by means of temperature increase is, evidently, stipulated by reduction of the solid carbide-cementite phase share in the deposited metal.

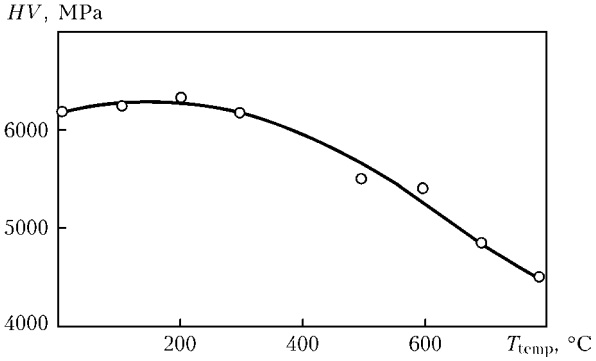

Figure 4. Influence of tempering temperature on hardness of deposited metal

So, on basis of the results obtained one may state that tribotechnical characteristics of mating arrangement 2 may be improved by means of heat treatment of the deposited metal at T_{temp} = 520–550 °C. Increase or reduction of the temperature is accompanied by worsening of the friction pair serviceability parameters, whereby maximum wear resistance of both the deposited metal and a mated with it insert is ensured by achievement of optimum quantitative ratio between two main phases of its structure.

1. Krivchikov, S.Yu., Zhudra, A.P., Petrov, V.V. (1994) Current technologies of arc hardfacing of crankshafts. *Svarochn. Proizvodstvo*, **5**, 4–6.
2. Zhudra, A.P., Krivchikov, S.Yu., Petrov, V.V. (2006) Effect of silicon on properties of low-alloy carbon deposited metal. *The Paton Welding J.*, **8**, 43–44.

ON ISSUE OF BRAZING METALS USING POWDER BRAZE ALLOYS OF DIFFERENT DISPERSITY

A.S. PISMENNY, V.I. SHVETS, V.S. KUCHUK-YATSENKO and **V.M. KISLITSYN**
E.O. Paton Electric Welding Institute, NASU, Kiev, Ukraine

The paper presents results of investigations of copper and brass joints made using silver powder with less than 1 μm particle size as the braze alloy. Explanation is given of abnormally high formation rate of the seam melt of eutectic composition in brazing. Application of powders with higher degree of dispersity has good prospects for joining structural materials for which heating temperature is critical.

Keywords: brazing, powder braze alloy, silver, dispersity, brazing temperature, process activation

At present new composite despersion-strengthened and other metal-base materials are used insufficiently widely because of absence of reliable methods for their joining. Because of this reason development of the joining methods which would not be inferior to the existing ones in respect to productivity and quality is an actual issue.

In application of welding or high-temperature brazing processes an important and not completely solved issue is loss of strength of the materials being joined in the heat-affected zone.

One of efficient methods of reducing brazing temperature became application as filler materials of amorphous films and nanolayer foils which, as it is known, interact more actively in comparison with traditional braze alloys [1, 2] with the base metal.

In a number of works reduction of the melting point of the materials, dispersed down to the nanosize level, is noted [3, 4]. Of interest is application of this phenomenon for reduction of the brazing temperature. Up till now investigations in these directions were not carried out which was, evidently, connected with instability of properties of fine-dispersed metal powders.

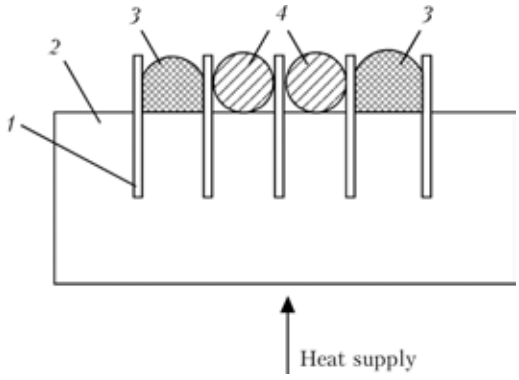

Figure 1. Scheme of copper substrate heating: *1* — spacers from mica plates; *2* — copper substrate; *3, 4* — silver powder with size of particles respectively less than 1 μm and more than 100 μm in mixture with F284 braze flux

The goal of this work consisted in technological check of possibility of reducing of the copper and brass brazing temperature due to dispersity increase of the powder braze alloy.

It is known that in brazing of copper and brass using silver due to contact melting a molten phase is formed which plays part of the braze alloy. Its composition corresponds to composition of eutectics of the Cu–Ag system with melting point 779 °C [5]. In contact melting of brass and silver the eutectic phase of the Cu–Ag–Zn triple system is formed which has melting point below 700 °C [6]. For intensification of diffusion interaction of the contacting metals the brazing temperature should exceed melting point of the eutectics.

In the experiments copper of the M1 grade, brass of the LS68 grade, and silver of commercial purity were used. A monodispersed silver powder with particles less than 1 μm was produced under laboratory conditions by means of anode dissolution, and more course fraction — by mechanical comminuting.

The experiment was carried out as follows: on peripheral areas of the copper substrate shots of silver powder with size of the particles less than 1 μm, and on central areas — more than 100 μm — were applied (Figure 1). Silver powder was used in mixture with the F284 flux. Silver powder shots were arranged between mica plates at distance 0.5 mm from each other.

Heating was performed using hydrogen-oxygen flame in center of the copper substrate from its lower side. Presence on the copper substrate of dividing grooves of up to 3 mm depth allowed creating temperature field from center to periphery of the substrate with the gradient not less than 50 deg / mm. So, course fraction powders were subjected to heating up to the temperature which was by more than 50 °C higher than temperature of the powder shots with particle sizes less than 1 μm.

Process of the silver powder melting in heating was controlled using the MBS-2 optical microscope (magnification power equals 32).

The experiments showed that in heating after melting of the flux first formation of the molten metal phase on the contact boundary of the copper substrate

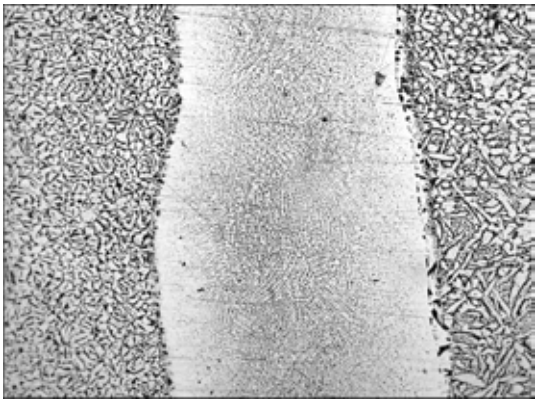

Figure 2. Joint microstructure of specimens from brass brazed using silver powder with particles of less than 1 μm size (×100)

with the silver powder, which had size of the particles less than 1 μm, occurred. On contact boundary with coarser silver particles the molten metal phase is formed in significant volumes only at heating to a higher temperature. Time delay of the contact melting of the powder with a coarser fraction equals about 5 s. According to readings of the thermocouples, at the time of melting of the powder with a coarser fraction temperature in this area is by more than 50 °C higher than temperature of the area with silver powder of finer fraction.

In our opinion intensification of the contact melting in case of comminution of silver particles is stipulated by significant increase of the silver powder contact surface — main component of the melting process. In addition to increase of the contact surface area with the copper substrate, bringing of silver to the contact boundary occurs due to diffusion and mass transfer in the flux melt. Probably, in this case more complex processes occur that require for further investigations. As a version one may assume that reduction of the silver melting point occurs due to comminution of its particles down to the size less than 1 μm.

Possibility of practical implementation of the observed effect was checked in brazing of specimens from copper and brass. On specimens of 30 × 5 × 0.3 mm size a braze alloy material was applied, which represented mixture of the F284 flux and silver with size of particles less than 1 μm. The specimens were lapped, compressed between two rods from ceramics using force up to 3 N, and subjected to heating by a hydrogen-oxygen flame.

It was established that formation of the joints at heating within approximately 30 s occurred at the temperature close to the eutectic one, while at brazing using traditional braze alloys of the Ag–Cu system, for example a standard PSr72 braze alloy, it was necessary to heat specimens up to the temperature, which was by more than 50 °C higher than the eutectic one [6].

Investigation of the microstructure and chemical inhomogeneity of brazed joints of the specimens from brass and copper, produced with application of silver powder with particles of less than 1 μm size, were carried out using the optical microscope «Neophot-32» and the Camebax microanalyzer SX-50.

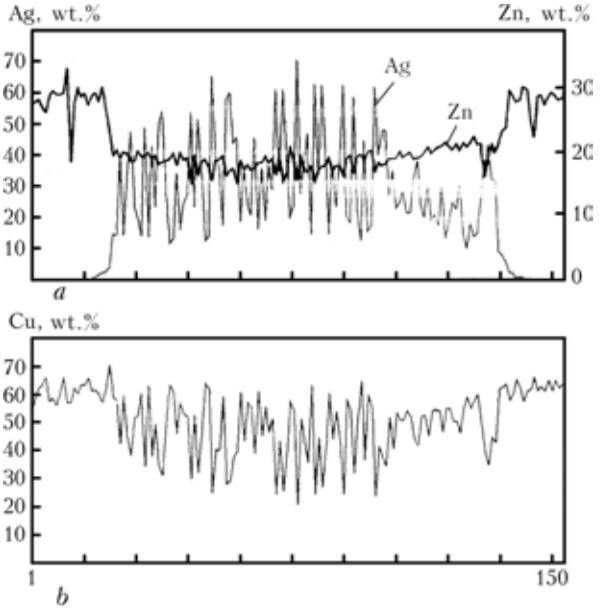

Figure 3. Distribution of silver, zinc (*a*) and copper (*b*) in joint of specimens from brass brazed using silver powder with size of particles less than 1 μm (length of area — 750 μm; step — 49.7 μm)

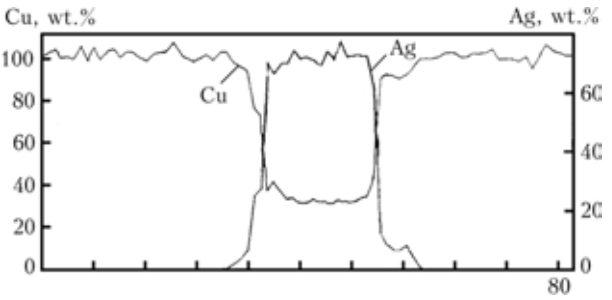

Figure 4. Ditribution of copper and silver in joint of specimens from copper brazed using silver powder with size of particles less than 1 μm (length of area — 80 μm; step — 10.1 μm)

Microstructure analysis of joints of specimens from brass (Figure 2) showed that phase transformations did not occur in HAZ. Metal of the brazed seam had a homogeneous fine-dispersed structure, and proceeding from distribution of the elements (Figure 3) represented an alloy of eutectic composition of the Cu–Ag–Zn system. Width of the brass diffusion zone was about 15 μm.

Distribution of copper and silver in copper joints (Figure 4) also proved formation in a brazed seam of a fine-dispersed alloy of eutectic composition. The diffusion zone width of silver in copper did not exceed 7 μm.

Comparative tensile tests of specimens from copper and brass, brazed using silver powder with size of particles less than 1 μm and the PSr72 braze alloy, showed that mechanical properties of produced joints were practically identical.

CONCLUSIONS

1. Application of silver powders with size of particles less than 1 μm allows reducing temperature of contact-reactive brazing of copper and brass not less than

by 50 °C, as well as time of the braze alloy melt formation.

2. Activation of the melting process at increase of the powder braze alloy dispersity is stipulated by increase of the silver powder surface as the main component of the contact melting process and intensification of mass transfer in the flux melt.

3. Application of powders with high degree of dispersity as the braze alloy materials has good prospects for joining thermally unstable structural materials.

1. Ishchenko, A.Ya., Falchenko, Yu.V., Ustinov, A.I. et al. (2007) Diffusion welding of finely-dispersed AMg5 / 27 % Al_2O_3 composite with application of nanolayered Ni / Al foil. *The Paton Welding J.*, **7**, 2–5.
2. Kuchuk-Yatsenko, V.S., Shvets, V.I., Chvertko, P.N. et al. (2004) Flash-butt welding of dispersion-hardened copper alloy of Cu–Al_2O_3 system. *Ibid.*, **11**, 2--4.
3. Bogdanov, K.Yu. (2008) *Why nanoparticles melt at low temperatures?* http:www.nanometer.ru / 2008 / 02 / 9 / nanjchastici_temperature_plavlenia_60-57.html
4. Zhang, M., Efremov, M.Yu., Schiettekatte, F. et al. (2000) Size-dependent melting point depression of nanostructures: nanocalorimetric measurements. *Phys. Rev. B*, 62(**15**), Oct., 10548–10557.
5. Khryapin, V.E. (1981) *Reference book of tinman*. Moscow: Mashinostroenie.
6. (1984) *Reference book on soldering*. Ed. by I.E. Petrunin. Moscow: Mashinostroenie.

THESES FOR A SCIENTIFIC DEGREE

E.O. Paton Electric Welding Institute, the NAS of Ukraine

A.S. Milenin (PWI) defended on 8 of October 2008 candidate's thesis on topic «Kinetics of thermomechanical processes in braze-welding of titanium-aluminium beam structures».

The thesis was devoted to investigation of characteristic peculiarities of kinetics of thermomechanical state of titanium-aluminium beam structures in process of their braze-welding for the case of development and optimization of the production cycle of dissimilar structural elements of aviation designation (guides of armchairs). On basis of results of numerical and experimental investigations influence of technological parameters of the braze-welding process was determined on peculiarities of formation of stress fields in the area of dissimilar contact and on strained state of a beam structure after welding. Character of change of residual stress-strain state of dissimilar structures after heat treatment and machining of different kinds was determined.

Methodology for assessing risk of formation of intermetallic compounds in the area of the surface contact of molten aluminium with solid titanium was further developed. Physical explanation of the processes at initial stage of the braze-welding contact formation was made. Universal methodology for assessing risk of formation of embrittlement intermetallic inclusions as a result of reaction diffusion in variable and inhomogeneous temperature field in the area of the surface contact of titanium with aluminium was developed. This allowed determining character of influence of the welding heat source on risk of formation of this kind of defects in case of braze-welding of the titanium-aluminium beam aviation structures.

Peculiarities of the metal plastic strain kinetics in the process of braze-welding of structures from titanium and aluminium from the viewpoint of risk of the hot crack formation in aluminium part of the dissimilar joint were detected. Increased risk of the cross hot crack formation in the weld metal of a dissimilar braze-welded joint was demonstrated.

For efficient analysis of the numeric investigation results the computer means for modeling thermomechanical processes in braze-welding and post-weld treatment of titanium-aluminium beam structures were included into the problem-oriented software package.

Complex of investigations for determining input parameters of the developed models was carried out, which allowed obtaining efficient means for computer modeling of thermomechanical processes in dissimilar items. The data, obtained using modeling experiments, correlate with high accuracy with results of respective numeric investigations.

On basis of numeric analysis of results of thermomechanical processes in braze-welding and post-weld treatment of titanium-aluminium guides of armchairs were determined optimum technological parameters of these production cycles. Numeric investigations of influence of variation of the braze-welded double tee beam structure geometric parameters, in particular position of the dissimilar butt joint, on residual strains of the item bend allowed determining optimum ratio of titanium and aluminium parts of the double tee profile wall. Developed methodologies for assessing risk of forming defects of a dissimilar structure made it possible to specify allowable ranges of variation of the welding technological parameters

from the viewpoint of minimization of the risk of occurrence of embrittlement intermetallic layers and hot cracks.

Influence of postweld treatment of different kinds (local and general heat treatment, mechanical dressing) on residual stresses in the dissimilar contact area and shape of a dissimilar beam structure was investigated. Optimum technological parameters of these processes were determined.

On basis of results of the carried out investigations scientifically substantiated additions to technological recommendations were developed.

A.S. Zatserkovny (PWI) defended on 8 of October 2008 candidate's thesis on topic «Modeling of heat exchange processes of low-temperature plasma jet with evaporating and exothermally reacting particles of a disperse material».

The thesis is devoted to theoretical investigation and mathematical modeling of thermal and dynamic interaction of the plasma jet with particles of the disperse materials under conditions of the plasma spraying of coatings. Theoretical models for calculating heat exchange of a particle being sprayed with multicomponent plasma by accounting for energy input of ion and electron heat flows and exothermal reaction between the composite particle components were suggested.

On basis of analysis of physical processes, proceeding in Knudsen plasma layer near surface of the particle being sprayed, analytical expressions for calculating densities of electron and ion currents from plasma on surface of a particle, the potential fall between the plasma and the particle, and electron and ion components of heat flow from the plasma into the particle, were obtained. Method for determining parameters of such plasma on external boundary of Knudsen layer, which enter into the obtained analytical expressions, was determined. Within wide range of temperature change of the undisturbed argon plasma and the aluminium particle surface temperature the numeric analysis of composition, temperature of electrons, and heavy component of the near-surface plasma was carried out, and respective values of heat flows into the particle were calculated.

Mathematical model of heat processes, which proceed in a composite particle at its heating in the plasma jet, taking into account exothermal reaction of the intermetallic compound synthesis within its volume, was developed.

Calculation algorithms were found and respective software was developed using which a detailed computer modeling was carried out of movement and heating of both homogeneous (metal) evaporating and composite exothermally reacting particles in the plasma jet.

For the purpose of verification of the suggested mathematical models a series of full-scale experiments in spraying of Ni–Al composite powder were carried out. Using obtained experimental data parameters of the model of the composite particle movement were determined, and parameter, which characterizes rate of the exothermal reaction progress in their volume, was calculated. Suggested mathematical models of movement and heating may be adapted for wide range of the plasma spraying parameters and composite powders of different composition and structure.

A.A. Pismenny (PWI) defended on 22 of October 2008 candidate's thesis on topic «Efficiency increase of power supply of machines for resistance spot welding».

The thesis is devoted to analysis of the power supply and control problems of machines for resistance spot welding (RSW). On basis of analysis the most promising directions for further works in this field were determined. The thesis contains systematized analysis of known power supply systems for RSW on basis of which were carried out theoretical and calculation assessments of the most promising systems.

High efficiency of the reactive power longitudinal compensation systems of single phase machines for RSW of low and medium power up to 1000 kV·A was proved. In comparison with conventional single-phase machines they have significantly higher power factor, ensure increased stability of electrodes and stability of quality of the joints within wide range of their specific resistances.

Methodology for calculating power factors and values of relative voltages and currents on basis of assigned values of the angle for switching-on the thyristor contactor at various values of active resistance of the load was developed. It was established using the new developed method of calculation that within the range of the thyristor switch-on angles up to 60 electrical degrees one may obtain high values of power factor cos φ (up to 0.95), deviation from full compensation in direction of under-compensation being 25 %.

Power supply system with a three-phase converter of the number of phases and 30 Hz frequency was recognized a promising one for the RSW machines of more than 100 kV·A power. Quasi-symmetrical work of the converter allows achieving close to uniform distribution of current over the network phases without loading of zero wire, while reduction of the working current frequency allows increasing the machine power factor cos φ by 20–30 % in comparison with traditional power supply system of the RSW machines of industrial frequency. In technological relation application of AC welding at reduced 30 Hz frequency will allow increasing acting value of current under load and reducing risk of partial melting of the welding electrodes and cases of the metal splashing out from the welding zone.

It was suggested to use for welding and microwelding of parts of small (less than 1 mm) and especially small (below 0.1 mm) thicknesses an inverter converter of increased frequency of welding current as alternative of the capacitor-type welding.

The work contains description of the developed design, manufacturing and testing of the experimental model of the inverter power supply source of increased current frequency 500 Hz for resistance spot microwelding in which a specially developed algorithm for automatic control of welding conditions is implemented. This power supply source ensures process of high-quality welding of items within thickness range 0.05–0.50 mm and simulates power supply source with the current frequency 30 Hz for welding of items within thickness range 5–8 mm.

New power supply source was successfully tested in welding of the carbon group metals with thickness of welded parts less than 1 mm. Quality of welded joints was positively appraised by leading enterprises of the country.

TECHNICAL WORKSHOP OF WELDING SPECIALISTS IN SIMFEROPOL

From 9 till 11 of September 2008 at Electric Machine Industry Plant of OJSC FIRMA SELMA and its recreation grounds «Parus» was held technical workshop of welding specialists on topic «State-of-the-art welding equipment and advanced technology of welding in ship building, ship repair, crane building and production of hoisting-transportation equipment». More than 30 specialists from enterprises and organizations of Ukraine (Chernomorsky Ship Building Plant; «Okean»; «Tekhnolazer-svarka» Ltd, Nikolaev; «Cranship»; Ship Repair Plant, Kerch; «Lazurit»; «Avrora» Ltd; FSUE-13, SRP «Yuzhny» Ltd, Sevastopol; OJSC «Azovmash»; STC «Promavtosvarka»; SRP Ltd, Mariupol; CJSC Crane Building Plant, Nikolaev; the E.O. Paton EWI; «Neftegazstrojizolyatsiya», Kiev; «Zaporozhkran»; OJSC «Zaporozhie Plant of Welding Fluxes and Glass Items»; «Arksel», Donetsk), 20 specialists from Russia (OJSC «Sevmash», Severodvinsk; Verkhnekamsky Ship Building Complex, Perm; «Institute BVIIST» Ltd, Moscow; «ITS»; SE «Admiraltejskie Verfi»; TsNIITS, St.-Petersburg; OJSC «Chelyabinsk Pipe-Rolling Plant»; «Elektrosvarka», Kaliningrad; «Vineta» Ltd, Nikolskoe) and representative of «Drahtzrug Stein Wire Welding», Germany, took part in the workshop. Managers and chief specialists of main services of SELMA and ITS also took part in the workshop.

In the assembly hall participants of the workshop were welcomed by director-general of FIRMA SELMA G.V. Pavlenko and director-general of ITS M.V. Karasyov. Technical director S.I. Gritsenko and D.N. Rabochinsky presented brief information.

Then tour of main and support workshops and bays of the plant was made where S.I. Grishchenko and M.V. Karasyov acted as guides.

Success of the enterprise in expansion and upgrading of the production nomenclature, improvement of manufacturing technology, application of well organized quality assurance system literally at each working place, correctly organized saving regime of the resources, incentive system of labor payment, and attention paid to social issues made deep impression. As a result, significant growth of production, expressed, for example, in volumes of the equipment sales, is observed. It achieved 12–13 mln UAH per month. The plant plans to open Trade house, which will allow activating marketing activity of the enterprise.

At present SELMA is a dynamically developing enterprise, assortment of equipment of which constitutes more than 100 names of welding equipment: welding transformers, rectifiers, semi-automatic machines, welding automatic machines and carrying structures for mechanization of welding and cutting, installations for air-plasma cutting, machines for resistance spot welding and equipment for controlling spot welding machines, and equipment for mechanical preparation of edges for welding. List of produced equipment constantly expands due to development of new kinds of welding equipment which meets state-of-the-art requirements of production and application of latest achievements of science and technology.

A number of reports were presented at the workshop within two days. Block of presentations of the SELMA specialists included the following papers: «General review of produced products. New items. Promising directions of the welding equipment development at SELMA. Welding converters of the KSU type» (chief designer G.L. Pavlenko); «Welding automatic machines for welding and surfacing. Promising directions of the equipment development for automatic welding at SELMA (V.A. Pankratiev); «Machines for mechanical preparation of edges for welding of the MKS and the MKF types» (V.A. Kozarin).

G.L. Pavlenko characterized main kinds of produced by SELMA products, dwelled in detail upon new developments, for example, the VS-450 rectifier (analogue of Varco star 400), universal sources with choppers for manual and semi-automatic gas-shielded and TIG welding, welding converters of the KSU type, welding automatic machines and automatic heads, structures for automation of welding processes (GK-200 «Proteus» etc.). In future it is planned to produce automated complexes for air-plasma cutting, equipped with the SELMA sources.

SELMA started production of welding automatic machines in 1999, having taken as basis automatic machines of the A2 and A6 type (ESAB). They include the ADF-1000 and the ADF-1250 automatic machines with smooth or staged regulation of the welding wire feeding of 2–5 mm diameter.

Edge-spalling machines, produced by SELMA, ensure minimal (close to zero) tolerance in processing of edges and rate of processing more than 2 m / min. They have no disadvantages peculiar for Italian machines (small service life of the reduction gearbox). There is positive experience of using the MKS 214 machine at Volzhsky Pipe Plant.

In report of M.V. Karasyov (ITS) activity of the group of enterprises, which enter into ITS, was presented. The group includes SELMA company, OJSC ESVA (Kaliningrad), «Welding» Ltd. (Lithuania), representative offices and warehouses (Ekaterinburg –– ITS-Ural; Krasnoyarsk –– ITS-SIBIR, ITS-VOLGA; Samara, Moscow –– ITS MOSCOW, ITS-ENGINEERING, Irkutsk–welding equipment–Irkutsk, etc.), and industrial-warehouse complex PARNAS (St.-Petersburg).

Group of the ITS enterprises annually produces and delivers more than 80 thou units of welding equipment in territory of Russia, more than 50 thou units in territory of Ukraine, more than 2 thou welding installations are supplied far abroad.

All together volume of production constitutes more than 149 thou units of welding equipment. Nomenclature of the items constitutes more than 80 names. Share in CIS among Russian companies constitutes up to 75 % of the whole national welding equipment operating in territory of Russia. Share in CIS among whole welding equipment of Russian and foreign companies is about 50 %.

General number of employees at all ITS enterprises is 1700. The company has its own recreation grounds «Parus» near Evpatoriya. Production department of ITS in St.-Petersburg specializes in completion on order of automated installations for industrial needs with application of standard equipment of SELMA and other companies.

From new kinds of equipment of the ITS enterprises M.V. Karasyov noted high reliability of welding converters (choppers), their high efficiency, which achieves 93 %, and low power consumption. There are good prospects for their application in ship building. One of advantages of using choppers is achievement of reduced content of hydrogen in the weld metal. Experimental data are available which prove that application of the converters in composition of the VDU-1500 multipost source (8 converters) in multiarc welding using flux-cored wire allows obtaining fine-grain structure of the weld metal in welding of pipe steels. According to data of the speaker, application of the KSU-320 converter allows ensuring high efficiency of its use due to reduction of power consumption, reduction of sputtering in welding, and high technological properties. Among novelties of the equipment, which are widely used in recent years, the speaker noted the VDU-511 and VD-506DK rectifiers, the installations for automatic submerged-arc welding VDU-1500 (direct current) and TDFZh-1250 (alternating current). Production of welding complex PROTEUS (TU 3441-028-11143754–2006) deserves attention. It is designed for automatic gas-shielded or gas mixture-shielded orbital welding of position joints of pipelines of 406–2540 mm diameter. It includes: two self-propelled welding heads, a power unit, a guiding belt of 120 mm width, a manual programming device (12 programs), a remote control panel, a set of appliances and replaceable parts, and a welding current source (VD-506DK UZ).

At the workshop presentations of TsNIITS specialists were also made: N.A. Steshenkova «Development of civil ship building within framework of FTsP for 2009–2016. Prospects of building of ships of new generation, including gas carriers» and «Innovation technologies of welding suggested for mastering within framework of FTsP of civil ship building development»; V.A. Nikitin «Application of robots for welding of ship structures».

The floor was given also to S.V. Golovin (VNIIST) who made report «Quality of welded structures –– the base for increasing reliability, working life and competitiveness of ship building»; A.N Alimov (Arksel) «Production of seamless flux-cored wires»; A.I. Romantsev (OJSC ChTZ) «New pipe electric welding workshop»; R.N. Barannik (Zaporozhie Plant of Welding Fluxes and Glass Items) «Mastering of production of new kinds of ceramic fluxes».

Participants of the workshop expressed their gratitude to representatives of SELMA and ITS for excellently organized work of the workshop, its saturated program, and satisfaction with level of presented reports.

Prof. V.N. Lipodaev, PWI

CONFERENCE «BRAZING-2008» IN TOLIATTI

On 10–12 of September 2008 International Conference on Brazing was held in Toliatti –– the highest forum in CIS in this field. Sixty papers from Russia, Ukraine and Germany were presented at the conference.

At plenary meeting great attention was attracted by presentations made by V.S. Novosadov (Moscow University of Food Production) «Phenomenological theory of boundary and diffusion kinetics of solution in capillary gap»; V.F. Khorunov (E.O. Paton Electric Welding Institute, Kiev) «Brazing of intermetallic alloys. Achievements and problems»; V.N. Semyonov (SPA «Energomash», Khimki) «Model of physical-chemical interaction of the EP202 alloy with copper-silver braze alloy and strength of their bond at interface»; L.S. Lantushenko (OJSC «Kriogenmash», Balashikha) «Fluxless brazing of aluminium alloys». These reports generalized results of long-term investigations in the field of theory of the metal material joining, prospects of using intermetallic compounds as structural materials, manufacturing of missile engines, achievements in the field of fluxless brazing of aluminium alloys.

Interesting information (TSU, Toliatti) contained reports of L.V. Loshkaryov «On possibility of acoustic-emission control of metals and compounds», and of D.L. Merson «New method of NDT of phisical-mechanical properties of metals and joints». A pleasant decoration of the plenary meeting became demonstration of achievements of the jewelry art chair of Toliatti State University.

Doubtless success of the organizers was arrangement within the framework of the conference of the seminar «State-of-the-art welding equipment and technology of welding and brazing of the Abicor Binzel groups». Six presentations were made with subsequent demonstration of spot plasma welding and manual plasma brazing with application of the SBI source and the ABICOR torch; robotized welding and brazing with application of the FANUC robot, the KEMPPI power source and the ABICOR torch; braze-welding process of galvanized parts on the KEMPPI apparatus Pro Evolution. This is a very bright demonstration of close cooperation of Russian specialists with Western companies.

One more prove of this is significant number (7) of presentations from Germany in addition to those made at the seminar. One has to single out from these presentations works, carried out under management of Prof. J. Wilden. So, in paper «New technology for joining sensitive to heating materials» were presented results of investigations of the joints produced with application of «cold arc» (cold metal transfer), hybrid process (cold arc plus laser) in joining, for example, of steels, aluminium with steel, whereby zinc-base alloy was successfully used as a braze alloy. In the work «Nanotechnology and boundary effects as new possibilities for successful joining of materials» interesting results of investigations of the joints produced with application of nanomaterials were presented. As basis for such experiments the data published in works of Soviet scientists were used.

Rather interesting was presentation of V.E. Soshkin et al. «State-of-the-art efficient fiber refractory materials for high-temperature insulation of non-organic binders» which suggested new ways for solution of thermal insulation issues, in particular, in vacuum furnaces.

Big number of interesting presentations were made by employees of TSU. Among them one has to note work of R.S. Luchkin «Diffusion model of reliability of brazed units of copper alloys under conditions of electrochemical corrosion», presentations made by A.Yu. Krasnopevtsev «Brazing of high-alloy steels in low vacuum and argon» and B.N. Perevezentsev «Influence of alloying elements on mechanical properties of titanium structures brazed with aluminium-base braze alloys». The latter work is important from the viewpoint of serial production of titanium honeycomb structures.

Actively works in Russia (Moscow) «Union of professional brazing operators» under management of I.N. Pashkov. On behalf of this Union a number of papers were presented which mainly concerned their particular issues, but, undoubtedly, containing useful information for the industry. One has to especially note efforts of this Union in organization of training process in higher educational institutions of Russia with specializing in brazing (with participation of V.S. Novosadov). It is known that invaluable contribution in this field was made by employees of TSU. This experience will be used on all-Russia scale.

It should be noted that in Russia continue to actively work such companies as Alarm, MIFI-Ameto (Moscow) which ensure provision of Russian enterprises with braze alloys on different bases for wide range of materials. In papers on behalf of these companies their latest achievements were reflected.

Low-temperature brazing was presented at the conference by informative presentations of E.S. Nazarov (SPE «KVP Raduga» Ltd, Moscow) and N.P. Litvinenko (FSUE SPE «Istok», Fryazino).

Assessing work of the conference as a whole, one should note increased activity of Russian specialists in this field, appearance of a big galaxy of scientists and production workers which occupy leading positions in development of braze alloys, fluxes, technologies, and preparation of training programs. Still there are few fundamental works carried out with involvement of state-of-the-art methods of investigations, but available scientific potential will allow doing this in near future, moreover that active interaction of Russia and Europe is evident.

One can not but note good, as usually, organization of the conference, exceptional kindness to guests of the TSU employees. One wishes to express them big gratitude and further successes.

V.F. Khorunov, Cor.-Member of the NAS of Ukraine, PWI

INDEX OF ARTICLES FOR TPWJ'2008, Nos. 1–12

NEWS

NON-DESTRUCTIVE TESTING

PLENARY PAPERS FOR INTERNATIONAL CONFERENCE ON WELDING AND RELATED TECHNOLOGIES INTO THE THIRD MILLENNIUM

SCIENTIFIC AND TECHNICAL

LIST OF AUTHORS